UNIVERSITY OF CALIFORNIA SAN DIEGO

A Genome-wide CRISPR Screen Reveals a Role for the Non-canonical Nucleosome-Remodeling BAF Complex in Foxp3 expression and regulatory T cell function

A dissertation submitted in partial satisfaction of the requirements for the degree

Doctor of Philosophy

in

Biology

by

Chin San Loo

Committee in charge:

Professor Ye Zheng, Chair
Professor John T. Chang
Professor Diana C. Hargreaves
Professor Li-fan Lu
Professor Wendy Huang
Professor Elina Zuniga

2020

The Dissertation of Chin San Loo is approved, and it is acceptable in quality and form for publication on microfilm and electronically:

Chair

University of California San Diego

2020

DEDICATION

To my mother, who selflessly encourages me to go abroad and follow my dreams.

To my love, thank you for supporting me in every stage of my life.

EPIGRAPH

"Discovery consists of looking at the same thing as everyone else and thinking something different."

Albert Szent-Györgyi

TABLE OF CONTENTS

LIST OF FIGURES

LIST OF SUPPLEMENTAL FILES

ACKNOWLEDGEMENTS

I want to thank Ye for his mentorship over the years, allowing me to explore, to learn, and to grow as an independent researcher. I also want to thank Lyn and Diana for seamless and fruitful collaboration. Lastly, I want to thank my committee for their insights, advice and suggestions, which have helped in shaping my project and my career development.

I was supported by the Albert G. and Olive H. Schlink Foundation. Jovylyn Gatchalian was supported by the Salk Institute T32 Cancer Training Grant T32CA009370 and the NIGMS NRSA F32 GM128377-01. Diana C. Hargreaves was supported by the National Institutes of Health (GM128943-01, CA184043-03), the V Foundation for Cancer Research V2016-006, and the Leona M. and Harry B. Helmsley Charitable Trust. Ye Zheng was supported by the NOMIS Foundation, the Crohn's and Colitis Foundation, the Leona M. and Harry B. Helmsley Charitable Trust, and National Institute of Health (AI107027, AI151123, and OD023689). This work was also supported by National Cancer Institute funded Salk Institute Cancer core facilities (CA014195).

The contents and data presented in this dissertation is adapted from an article that was published in July 14th, 2020 in the journal of *Immunity*, titled "A Genome-wide CRISPR Screen Reveals a Role for the Non-canonical Nucleosome-Remodeling BAF Complex in Foxp3 Expression and Regulatory T Cell Function". The authorship is: Chin-San Loo, Jovylyn Gatchalian, Yuqiong Liang, Mathias Leblanc, Mingjun Xie, Josephine Ho, Bhargav Venkatraghavan, Diana C. Hargreaves, and Ye Zheng.

VITA

2009	Bachelor of Science, National Taiwan University, Taipei City, Taiwan Clinical Laboratory Sciences and Medical Biotechnology
2009-2010	Medical Technologist, Island Hospital, Penang, Malaysia
2012	Master of Science, National Taiwan University, Taipei City, Taiwan Biochemistry and Molecular Biology
2012-2015	Research Assistant, Academic Sinica, Taipei City, Taiwan
2020	Doctor of Philosophy, University of California San Diego, La Jolla, USA Biological Sciences

PUBLICATIONS

1. **Loo CS**, Chen CW, Wang PJ, Chen PY, Lin SY, Khoo KH, Fenton RA, Knepper MA, Yu MJ. Quantitative apical membrane proteomics reveals vasopressin-induced actin dynamics in collecting ducts. *Proc Natl Acad Sci U S A 110:17119-17124 (2013)*
2. Bloomekatz J, Singh R, Prall OW, Dunn AC, Vaughan M, **Loo CS**, Harvey RP, Yelon D. Plateletderived growth factor (PDGF) signalling directs cardiomyocyte movement toward the midline during heart tube assembly. *Elife 2017 Jan 18;6. Pii: e21172 (2017)*
3. Chang C, **Loo CS**, Zhao X, Solt LA , Liang Y, Bapat SP, Cho H, Kamenecka TM, Leblanc M, Atkins AR, Yu RT, Downes M , Burris TP , Evans RM, Zheng Y. The nuclear receptor REV-ERB-a modulates Th17 cell-mediated autoimmune disease. *Proc Natl Acad Sci USA 116 (37), 18528-18536 (2019)*
4. **Loo CS**, Gatchalian J, Liang Y, Leblanc M, Xie M, Ho J, Venkatraghavan B, Hargreaves D, Zheng Y. A Genome-wide CRISPR Screen Reveals a Role for the Non-Canonical Nucleosome-Remodeling BAF Complex in Foxp3 Expression and Regulatory T Cell Function. *Immunity. 2020 Jul 1;S1074-7613(20)30266-1 (2020)*

ABSTRACT OF THE DISSERTATION

A Genome-wide CRISPR Screen Reveals a Role for the Non-canonical Nucleosome-Remodeling BAF Complex in Foxp3 expression and regulatory T cell function

by

Chin San Loo

Doctor of Philosophy in Biology

University of California San Diego, 2020

Professor Ye Zheng, Chair

Regulatory T cells (Treg) play a pivotal role in suppressing auto-reactive T cells and maintaining immune homeostasis. Treg development and function are dependent on the transcription factor Foxp3. Although a large body of work has been devoted to dissecting the molecular mechanisms regulating Foxp3 expression, a systematic, genome-wide approach has not been elucidated. In this study, we performed genome-

wide CRISPR loss-of-function screens to identify Foxp3 regulators in mouse primary Treg cells. The screen results not only confirmed a number of known Foxp3 regulators but also revealed many novel factors that control Foxp3 expression. Gene ontology analysis showed Foxp3 regulators were highly enriched in genes encoding subunits of the SWI/SNF nucleosome remodeling and SAGA chromatin modifying complexes. Among the three SWI/SNF-related complexes, the Brd9-containing non-canonical (nc)BAF complex promoted *Foxp3* expression, whereas the PBAF complex was repressive. Gene ablation or chemical-induced degradation of Brd9 led to reduced Foxp3 expression and reduced Treg function*. Brd9* ablation compromised Treg function in inflammatory disease and tumor immunity. Furthermore, Brd9 promoted Foxp3 binding and expression of a subset of Foxp3 target genes, indicating that Brd9 actively participates in the Foxp3-dependent transcriptional program. In summary, this work provides an unbiased analysis of the genetic networks regulating Foxp3 and reveal ncBAF as a target for therapeutic manipulation of Treg function.

CHAPTER ONE: INTRODUCTION

1.1 Discovery of Regulatory T cells

Regulatory T cells (Treg), characterized as CD4+ CD25+ Foxp3+ markers, are known as an immune suppressor that plays a vital role in maintaining immune system homeostasis by suppressing auto-reactive T cell response (Josefowicz et al., 2012; Sakaguchi et al., 2008). Historically, the idea of "Suppressor T cell" can be traced back to the early 1970s. Gershon and Kondo first reported that thymus-derived lymphocytes consisted of populations that not only facilitated but also inhibited immune responses, suggesting there were distinct cell populations that different from helper T cells may contribute to the immune suppressive effect (Gershon and Kondo, 1970). Since then, "Suppressor T cells" had been proposed and extensively investigated over the next decade, and a complex of T cells interacting cascades and soluble factors were described (Green et al., 1983). However, in the early 1980s, such a notion collapsed abruptly due to the lack of evidence of I-J molecule in the putative suppressor T cells. The I-J MHC molecule had been thought to be associated with the immunosuppressive effect (Kronenberg et al., 1983). In addition, several other factors such as the lack of reliable maker for defining the suppressor T cells, ambiguity in the suppressive mechanisms, and identification of soluble anti-inflammatory cytokines (e.g. IL10 and TGF-β) gradually led to evolving an atmosphere that many immunologists dismissed using the word "Suppressor T cells" in interpreting the immunosuppressive effect (Germain, 2008; Sakaguchi, 2011).

Despite “Suppressor T cells” studies waned in the late 1980s, several immunologists remained tenacious in investigating the role of T cells in immune tolerance. There were several important studies that have contributed to the identification of suppressor T cells. In 1969, Nishizuka and Sakakura first showed that mice with neonatal thymectomy three day after birth developed the destruction of ovaries, which later showed it was caused by autoimmunity (Kojima and Prehn, 1981; Nishizuka and Sakakura, 1969). Transferring of CD4+ T cells and CD4+ thymocytes into neonatal thymectomy-induced mice was able to inhibit autoimmune disease (Sakaguchi et al., 1982). Given these observations, the next imminent question is to identify marker that can distinguish two CD4+ T cell populations responsible for immune response and tolerance, respectively. In 1985, Sakaguchi *et al* reported that transferring $CD5^{low}$ CD4+ T cells (depleted of $CD5^{high}$ population) to BALB/c athymic nude mice can develop autoimmune disease. Contemporary, Powrie *et al* and Morrissey *at al* independently reported that transferring of $CD45RB^{high}$ to immune-deficient mice induced intestinal bowel disease (Morrissey et al., 1993; Powrie et al., 1993). These prior observations had led to Sakaguchi *et al* published a landmark paper in 1995 showing that transferring of CD25+ depleted splenocytes to BALB/c athymic nude mice were able to induce autoimmune diseases, whereas co-transferring of CD4+ CD25+ T cells inhibited the autoimmunity, thus identifying CD4+ CD25+ T cells (confined to $CD5^{high}$ and $CD45RB^{low}$) are the immune suppressive T cells, which later coined as regulatory T cells (Treg) (Sakaguchi et al., 1995).

Identifying CD25 marker was useful to distinguish Treg from other T cell population, which enable scientists to isolate and investigate their properties such as their development (Asano et al., 1996; Suri-Payer et al., 1998) and suppressive mechanisms (Takahashi et al., 1998; Thornton and Shevach, 1998). However, it remained questionable because CD25 maker is also generally expressed in activated T cells and B cells(Ortega et al., 1984). In 2003, three groups independently published a breakthrough paper showing that Foxp3, a member of the Forkhead transcription factor family, is highly and specifically expressed in Treg (Fontenot et al., 2003; Hori et al., 2003; Khattri et al., 2003). Their findings clearly indicated that Treg is a specific cell lineage that controls immune tolerance and allows the field using Foxp3 to generate Treg-specific transgenic models to study Treg biology.

1.2 Development of Regulatory T cells

The transcription factor, Foxp3, is a critical gene that orchestrates the molecular processes involved in Treg differentiation and suppressor function (Zheng and Rudensky, 2007). A mutant mouse known as Scurfy that spontaneously develop autoimmunity phenotype was identified causing by Foxp3 mutation (Brunkow et al., 2001). Genetic studies also indicated Foxp3 mutation responsible for the human autoimmune disease known as Immune dysregulation, polyendocrinopathy, enteropathy, X-linked (IPEX) syndrome (Bennett et al., 2001; Chatila et al., 2000; Wildin et al., 2001). In addition, Foxp3 ablation leads to converting Treg into pro-inflammatory effector T cells(Kim et al., 2007; Lahl et al., 2007). Therefore, understanding the

regulation of Foxp3 expression is vital to understand the development and maintenance of Treg.

The regulation of Foxp3 has been intensively studied over the past few years. Studies have found that T cell receptor (TCR) and IL-2 signaling pathways play critical roles in Foxp3 induction(Chinen et al., 2016; Lee et al., 2012). TGF-β signaling is essential for Foxp3 induction in periphery-derived Treg and *in vitro* induced Treg, although its role in thymus-derived Treg development is still under debate (Chen et al., 2003; Liu et al., 2008; Ouyang et al., 2010). A number of downstream transcription factors regulate Foxp3 induction was also identified *in vitro* or *in vivo*, including Stat5a/b, Cbf-β/Runx1/3, Nfat1, Smad3/4, cRel, and Creb (Burchill et al., 2007; Kim and Leonard, 2007; Kitoh et al., 2009; Long et al., 2009; Rudra et al., 2009; Tone et al., 2008; Yang et al., 2008). However, compared to the large number of studies focused on the mechanism of Foxp3 induction, relatively less is known about the factors that maintain Foxp3 expression in mature Treg cells. In addition, an intronic enhancer in *Foxp3* named CNS2 (conserved non-coding sequence 2), also known as TSDR (Treg-specific demethylated region), is a key cis-regulatory element required for stable Foxp3 expression(Polansky et al., 2008; Zheng et al., 2010). CNS2 is heavily methylated in naive and activated conventional T cells by DNA methyl-transferase 1 (Dnmt1), and deletion of *Dnmt1* leads to aberrant expression of Foxp3 in conventional T cells(Josefowicz et al., 2009). Once Foxp3 expression is induced during Treg development, the CNS2 region is rapidly demethylated, opening it up for the binding of transcription factors(Polansky et al., 2008). Foxp3 can bind to CNS2, as well as an

additional upstream enhancer named CNS0(Kitagawa et al., 2017), and stabilize its own expression in a positive feedback loop(Feng et al., 2014; Li et al., 2014b).

Post-translational modifications (PTM) of the Foxp3 protein, including phosphorylation, acetylation, and ubiquitination, are also a crucial part of the regulatory circuit that controls Foxp3 function and stability (van Loosdregt and Coffer, 2014). For example, a pair of enzymes, ubiquitin ligase Stub1 and ubiquitin hydrolase Usp7, promote or inhibit degradation of Foxp3 via ubiquitination, respectively (Chen et al., 2013; van Loosdregt et al., 2013). Finally, intracellular metabolism, and specifically the metabolic regulator mTOR (mammalian target of Rapamycin), has emerged as a key regulator of Foxp3 expression and Treg function. Weakened mTOR signaling increases Foxp3 expression in iTreg *in vitro* (Delgoffe et al., 2009), whereas complete ablation of mTOR in Treg using genetic models compromises effector Treg homeostasis and function (Chapman et al., 2018; Sun et al., 2018). Despite these and other significant advances in understanding the molecular mechanisms regulating Foxp3, a comprehensive picture of the regulatory networks that control Foxp3 expression is needed to comprehend fundamental Treg biology.

1.3 Role of SWI/SNF Chromatin Remodeler in Regulatory T Cells

The mammalian SWI/SNF complex is a multi-subunit complex with a core ATPase protein, either SMARCA4 (BRG1) or SMARCA2 (BRM), that uses energy derived from ATP hydrolysis to remodel nucleosomes on chromatin. Mouse genetic studies have demonstrated that conditional knockout of *Smarca4* leads to impaired

differentiation of neural progenitor cells (Lessard et al., 2007; Wu et al., 2007), cardiomyocytes (Takeuchi et al., 2011), skeletal muscle (Zhang et al., 2011), and T lymphocytes (Gebuhr et al., 2003; Zhao et al., 1998). In addition, a previous report demonstrated that genetic deletion of *Smarca4* in Tregs using the Foxp3-Cre driver results in the development of a fatal inflammatory disorder reminiscent of Foxp3 mutant *scurfy* mice (Chaiyachati et al., 2013). The authors showed that while Treg development and Foxp3 expression was normal in *Smarca4* deficient Tregs, Treg function was nevertheless compromised due to impaired activation of TCR target genes, for example chemokine receptor genes in Tregs. This is consistent with the rapid association of SMARCA4-containing SWI/SNF complexes with chromatin following TCR activation in T cells (Zhao et al., 1998).

Biochemical studies have demonstrated that SMARCA4 is associated with both the canonical BAF complex (BAF) and Polybromo1-associated BAF complex (PBAF) (Xue et al., 2000; Yan et al., 2005). In addition, recent studies in embryonic stem cells (ESCs)(Gatchalian et al., 2018) and cancer cell lines (Alpsoy and Dykhuizen, 2018; Michel et al., 2018; Wang et al., 2019) have identified a BRD9-containing complex or GBAF complex (also referred to as non-canonical BAF or ncBAF), which contains several shared subunits including SMARCA4, but is distinct from the BAF and PBAF complexes. Apart from uniquely incorporating BRD9, the GBAF complex also contains GLTSCR1 or the paralog GLTSCR1L and lacks BAF- and PBAF-specific subunits ARID1A, ARID1B, ARID2, SMARCE1, SMARCB1, SMARCD2, SMARCD3, DPF1-3, PBRM1, BRD7, and PHF10. The distinct biochemical compositions of these three

SWI/SNF complex assemblies suggest functional diversity. However, it is not known which SWI/SNF complex assemblies are expressed in Tregs and the potential roles of specific SWI/SNF variants in regulating Foxp3 expression and Treg development have not been studied in depth.

1.4 Application of CRISPR/Cas9 for gene perturbation study

The genome editing technologies has advanced progressively in the past few years and provided many possibilities of directly targeting and modifying genomic sequences in all eukaryotic cells. These technologies are Zinc-finder nucleases (ZFNs), transcription activator-like effector nucleases (TALENs), and clustered regulatory interspaced short palindromic repeat/Cas9-based RNA-guided DNA endonucleases (CRISPR/Cas9)(Gaj et al., 2016). CRIPSR/Cas9 has particularly been utilized the most due to the ease and versatile of this technology(Jiang and Doudna, 2017). This technology uses bacterial Cas9 endonuclease and programmable guide RNA, which can be configured to target virtually all genomic sites, to knockout any target genes. The Cas9 can be directed by a guide RNA to the target site, causing DNA double-strand breaks (DSBs) and followed by nonhomologous end joining (NHEJ) repair, thus resulting in a random base insertion and/or deletion of the target site(Jiang and Doudna, 2017). Moreover, the advent of CRISR/Cas9 has adopted into a powerful genome-scale lost-of-function genetic screen, which utilize a pooled guide RNA library to identify genes that underlie phenotype of interest (Shalem et al., 2014). Therefore, it is an ideal genetic tool for systematically dissecting the regulation of Foxp3 in Treg.

CHAPTER TWO: RESULTS

2.1 Genome-wide CRISPR Screen in Natural Treg Cells Identifies Regulators of Foxp3

To screen for genes that regulate Foxp3 expression, we first developed a pooled retroviral CRISPR sgRNA library by subcloning an optimized mouse genome-wide lentiviral CRISPR sgRNA library (lentiCRISPRv2-Brie) (Doench et al., 2016) into a newly engineered retroviral vector pSIRG-NGFR (Figure 1A,B). This newly developed vector allowed us to infect mouse primary T cells efficiently and to perform intracellular staining for Foxp3 without losing the transduction surface marker NGFR after cell permeabilization (Figure 1C). In addition, the NGFR+ transduced cells can be enriched by anti-NGFR staining and magnetic bead isolation; therefore, minimizing execution time in FACS sorting. Using this library, we performed CRISPR loss-of-function screen on Treg cells to identify genes that regulate Foxp3 expression. We activated CD4+Foxp3+ Treg cells isolated from Rosa-Cas9/Foxp3Thy1.1 reporter mice (Liston et al., 2008; Platt et al., 2014) with CD3 and CD28 antibodies and IL-2 (Figure 2A). Treg cells were transduced 24 hours post-activation with the pooled retroviral sgRNA library at multiplicity of infection of less than 0.2 to ensure that transduced cells only receiving one sgRNA. NGFR+ transduced Treg cells were collected on day 3 and day 6 to identify genes that are essential for cell proliferation and survival. In addition, the bottom quintile (NGFR+Foxp3lo) and top quintile (NGFR+Foxp3hi) populations were collected on day 6 to identify genes that regulate Foxp3 expression. We validated the screen conditions by transducing Treg cells with sgRNAs targeting Foxp3 itself, as well as previously reported positive (Cbfb) (Rudra et al., 2009) and negative (Dnmt1) (Lal et al., 2009)

regulators of Foxp3 (Figure 2B-D). Guide RNA sequences integrated within the genomic DNA of sorted cells were recovered by PCR amplification, constructed into amplicon libraries, and sequenced with a NextSeq sequencer.

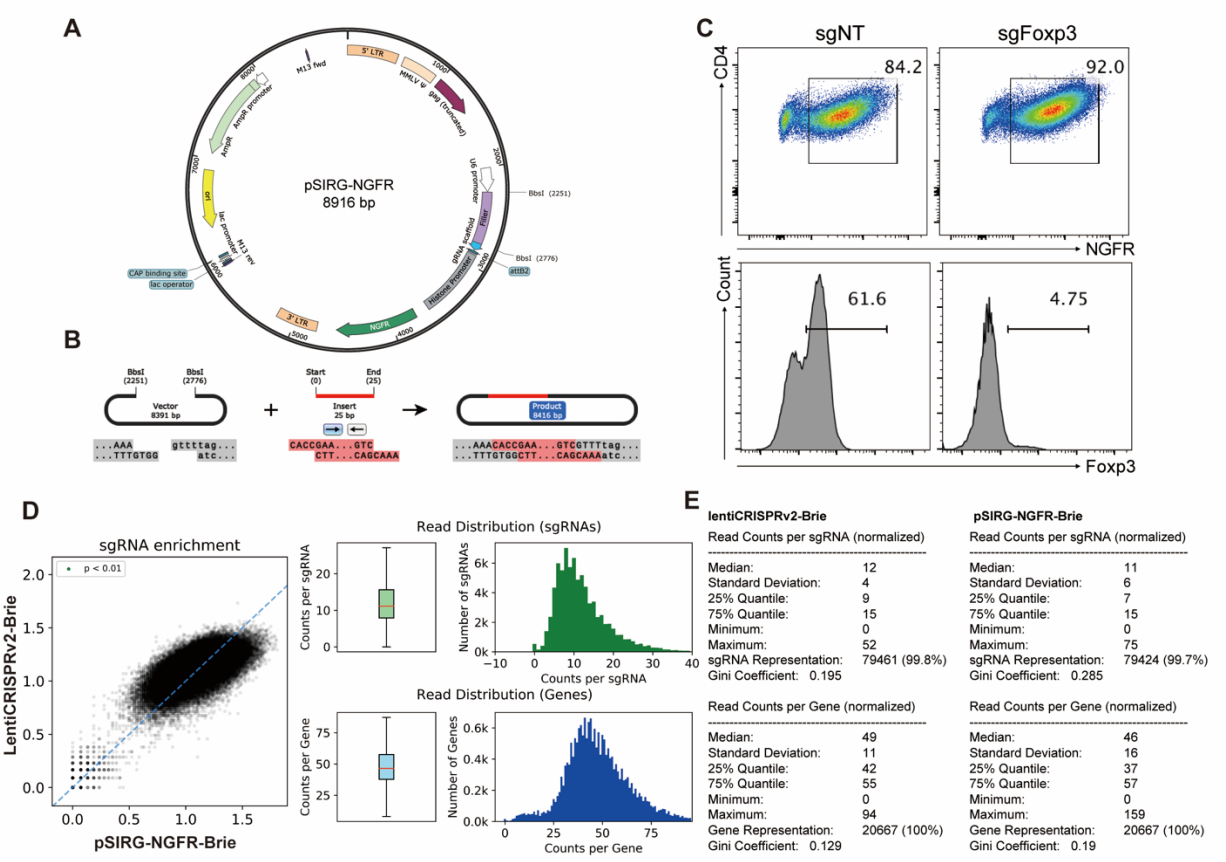

E

lentiCRISPRv2-Brie	
Read Counts per sgRNA (normalized)	
Median:	12
Standard Deviation:	4
25% Quantile:	9
75% Quantile:	15
Minimum:	0
Maximum:	52
sgRNA Representation:	79461 (99.8%)
Gini Coefficient:	0.195
Read Counts per Gene (normalized)	
Median:	49
Standard Deviation:	11
25% Quantile:	42
75% Quantile:	55
Minimum:	0
Maximum:	94
Gene Representation:	20667 (100%)
Gini Coefficient:	0.129

pSIRG-NGFR-Brie	
Read Counts per sgRNA (normalized)	
Median:	11
Standard Deviation:	6
25% Quantile:	7
75% Quantile:	15
Minimum:	0
Maximum:	75
sgRNA Representation:	79424 (99.7%)
Gini Coefficient:	0.285
Read Counts per Gene (normalized)	
Median:	46
Standard Deviation:	16
25% Quantile:	37
75% Quantile:	57
Minimum:	0
Maximum:	159
Gene Representation:	20667 (100%)
Gini Coefficient:	0.19

Figure 1. Construction of a retroviral sgRNA CRISPR vector and library.

A, The map of pSIRG-NGFR. A self-inactivating retroviral vector containing a sgRNA expressing cassette and a surface marker of truncated human nerve growth factor receptor (NGFR). **B,** Overview of the process to clone a sgRNA into pSIRG-NGFR. A pair of annealed sgRNA oligomers can be directly cloned into BbsI-digested pSIRG-NGFR by T4 ligation. **C,** Validation of the transduction and knockout efficiency of pSIRG-NGFR. Cas9-expressing naïve CD4 T cells were transduced with either non-targeting control virus (sgNT) or Foxp3 targeting virus (sgFoxp3) in the presence of TGF-β and IL-2 for Foxp3 induction. NGFR and Foxp3 expression were measured by FACS 3 days post-infection. **D,** Correlation of sgRNA representation comparing lentiCRISPRv2-Brie library to pSIRG-NGFR-Brie library (left). Read distribution of sgRNAs and genes in pSIRG-NGFR-Brie (right). **E,** Statistics of sgRNAs and genes represented in lentiCRISPRv2-Brie and pSIRG-NGFR-Brie. Quantification of sgRNAs and genes was computed by PinAPL-Py program.

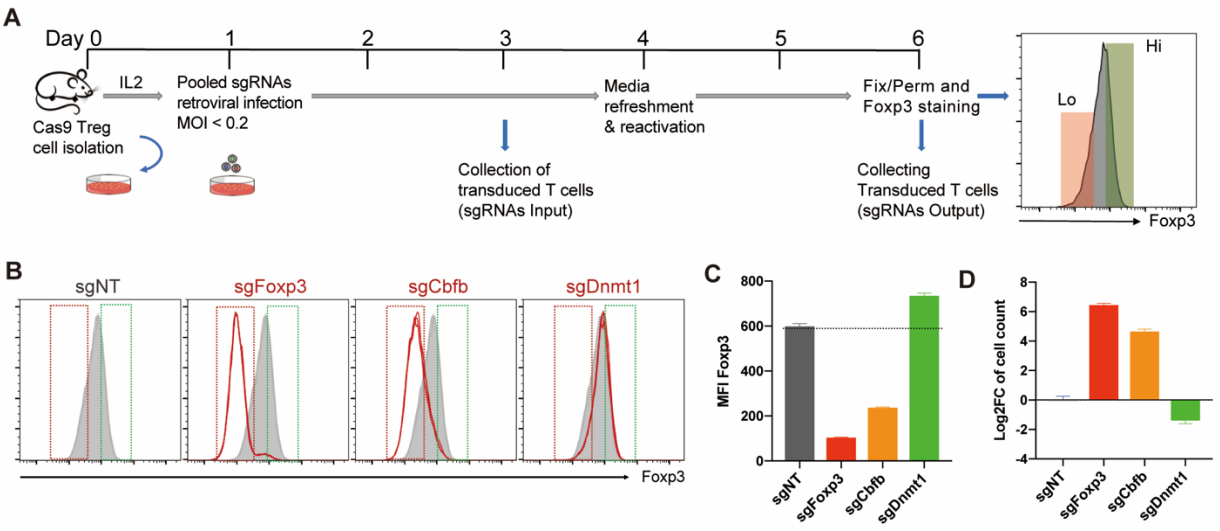

Figure 2. A genome-wide CRISPR screen in Treg cells.

A, Workflow of the CRISPR screen in Treg cells. **B-D,** Validation of the CRISPR screen conditions. **B,** FACS plots showing Foxp3 expression in Treg cells after sgRNA targeting of *Foxp3* (sgFoxp3), positive regulator *Cbfb* (sgCbfb), and negative regulator *Dnmt1* (sgDnmt1). Red and green gates were set based on Foxp3 low 20% and high 20% in sgNT Treg, respectively. **C,** Mean fluorescence intensity (MFI) of Foxp3 and **D,** Relative Log2FC of cell count comparing $Foxp3^{lo}$ to $Foxp3^{hi}$ after deletion of the indicated target gene (n=3 per group).

The relative enrichment of sgRNAs between samples and hit identification were computed by MAGeCK, which generates a normalized sgRNA read count table for each sample, calculates the fold change of sgRNA read counts between two cell populations, and further aggregates information of four sgRNAs targeting each gene to generate a ranked gene list (Li et al., 2014a). Prior to hit calling, we evaluated the quality of screen samples by measuring the percentage of mapped reads to the sgRNA library and total read coverage, which showed a high mapping rate (79.8-83.4%) with an average of 236X coverage and a low number of missing sgRNAs (0.625-2.5%) (Figure 3). With the cutoff criteria of log2 fold change (LFC) $>\pm 0.5$ and p-value less than 0.01, we identified 254 potential positive Foxp3 regulators enriched in the Foxp3lo population and 490 potential negative Foxp3 regulators enriched in the Foxp3hi population (Figure 4A,B and Supplemental Table 1). In a parallel analysis, we also identified 22 and 1497 genes that affect cell expansion and contraction, respectively (p-value < 0.002, LFC>1, Figure 4C,D and Supplemental Table 2). As expected, we identified genes belonging to pathways known to regulate Foxp3 expression both transcriptionally (Cbfb, Runx3) (Rudra et al., 2009) and post-transcriptionally through the regulation of Foxp3 protein stability (Usp7, Stub1) (Chen et al., 2013; van Loosdregt et al., 2013) (Figure 5A).

We next compared the potential positive and negative regulators with genes involved in cell contraction and expansion to exclude hits that might affect Foxp3 expression indirectly by affecting cellular fitness in general, leaving 197 positive Foxp3 regulators and 327 negative Foxp3 regulators (Figure 5B and Supplemental Table 3). Gene ontology analysis of positive Foxp3 regulators revealed a number of notable

functional clusters including SAGA-type complex, negative regulation of T cell activation, RNA Polymerase II holoenzyme, positive regulation of histone modification, and SWI/SNF complex (Figure 5C, Supplemental Table 4). Among negative Foxp3 regulators, genes are highly enriched in clusters related to negative regulation of TOR signaling, transcriptional repressor complex, mRNA decay and metabolism, and hypusine synthesis from eIF5A-lysine (Figure 5D, Supplemental Table 4). Several of these pathways, including mTOR signaling, Foxp3 ubiquitination/deubiquitination, and transcriptional regulation, have been implicated in Foxp3 regulation previously, suggesting that our screen is robust for the validation of known pathways and the discovery of additional regulators of Foxp3. Specifically, we identified many genes encoding subunits of the SAGA (Ccdc101, Tada2b, Tada3, Usp22, Tada1, Taf6l, Supt5, Supt20) and SWI/SNF (Arid1a, Brd9, Smarcd1) complexes (Supplemental Table 4), strongly suggesting that these complexes could have indispensable roles for Foxp3 expression. We thus further validated and characterized the SAGA and SWI/SNF related complexes to understand their roles in Foxp3 expression and Treg function.

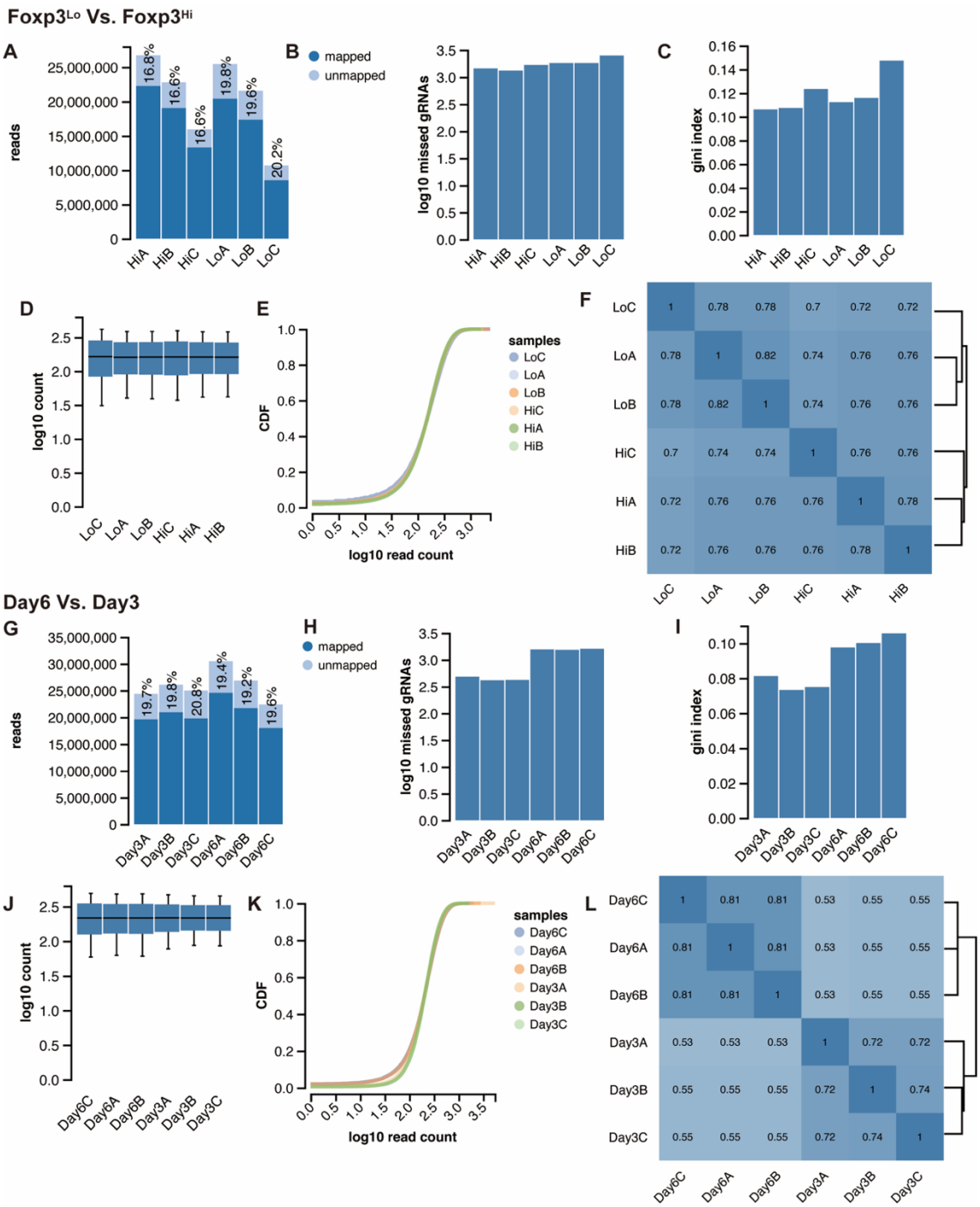

Figure 3. Quality control analysis of samples generated from the screen in Treg cells.

Quality control analysis of samples comparing between Foxp3Lo and Foxp3Hi populations **(A-F)** or between Day 6 and Day 3 NGFR+ transduced populations **(G-L). A, G,** Mapped (dark blue) and unmapped (light blue) reads for each sample. Percentage of unmapped reads is labeled on each bar. **B, H,** Number of missed gRNAs with zero mapped reads. **C, I,** Gini Index for each sample measuring inequality between read counts. **D, J,** Distribution of normalized read counts for each sample. **E, K,** Cumulative distribution function of normalized read counts for each sample. **F, L,** Correlation between normalized $\log_{10}$ read counts of samples.

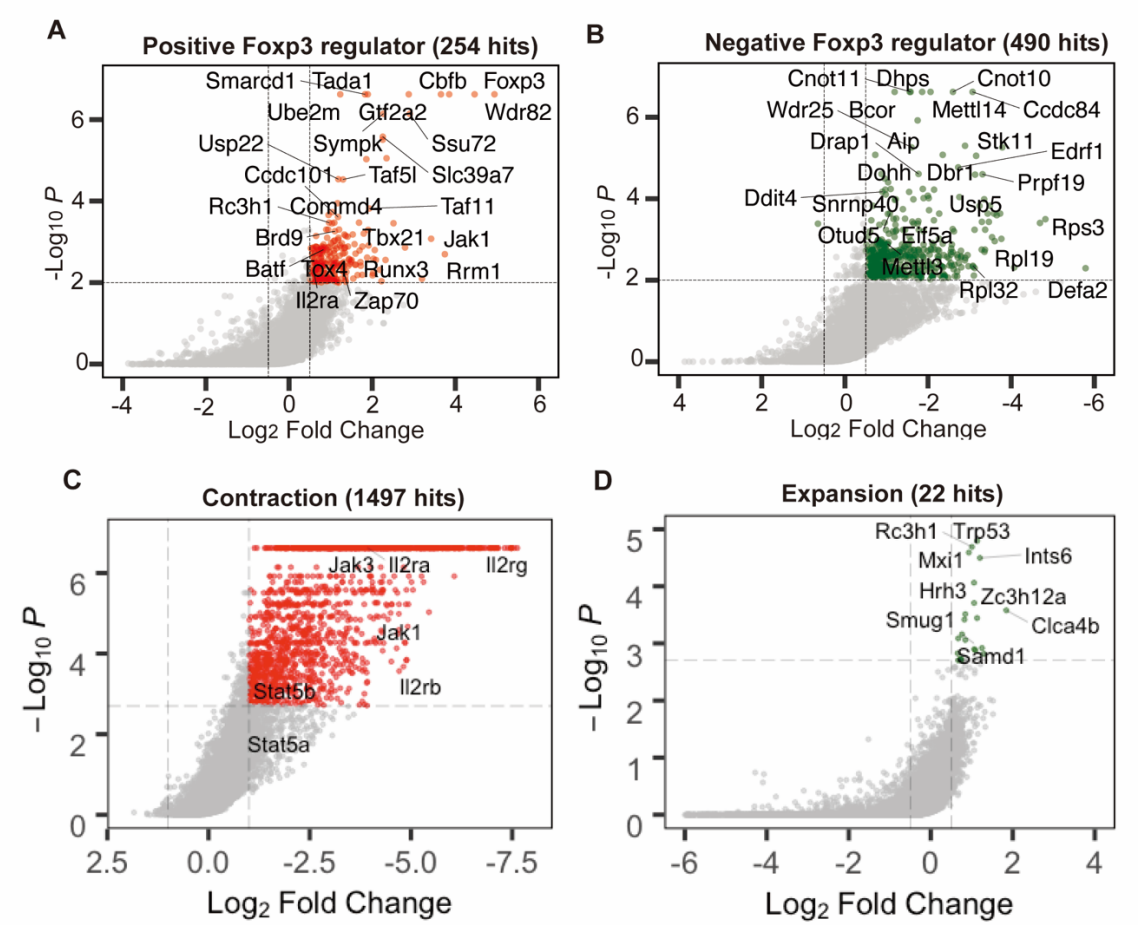

Figure 4. Identification of genes that regulated Foxp3 expression and cell proliferation/survival from the screen in Treg cells.

A, B, A scatter plot of the Treg screen result showing positive regulators **(A)** and negative regulators **(B)**. Genes that have met cutoff criteria (P-value<0.01, and Log2FC >± 0.5) are shown as red dots for positive regulators and green dots for negative regulators. **C,D,** A scatter plot showing genes enriched in the cell contraction pool **(C)** or cell expansion pool **(D)** by comparing NGFR+ transduced cells on day 6 to NGFR+ transduced cells on day 3 from the screen in Treg cells. Cutoff was set for contraction is P-value < 0.002 and LFC > 1 (**C,** Red dots), whereas cutoff for expansion was set P value < 0.002 and LFC > 0.5 (**D,** Green dots).

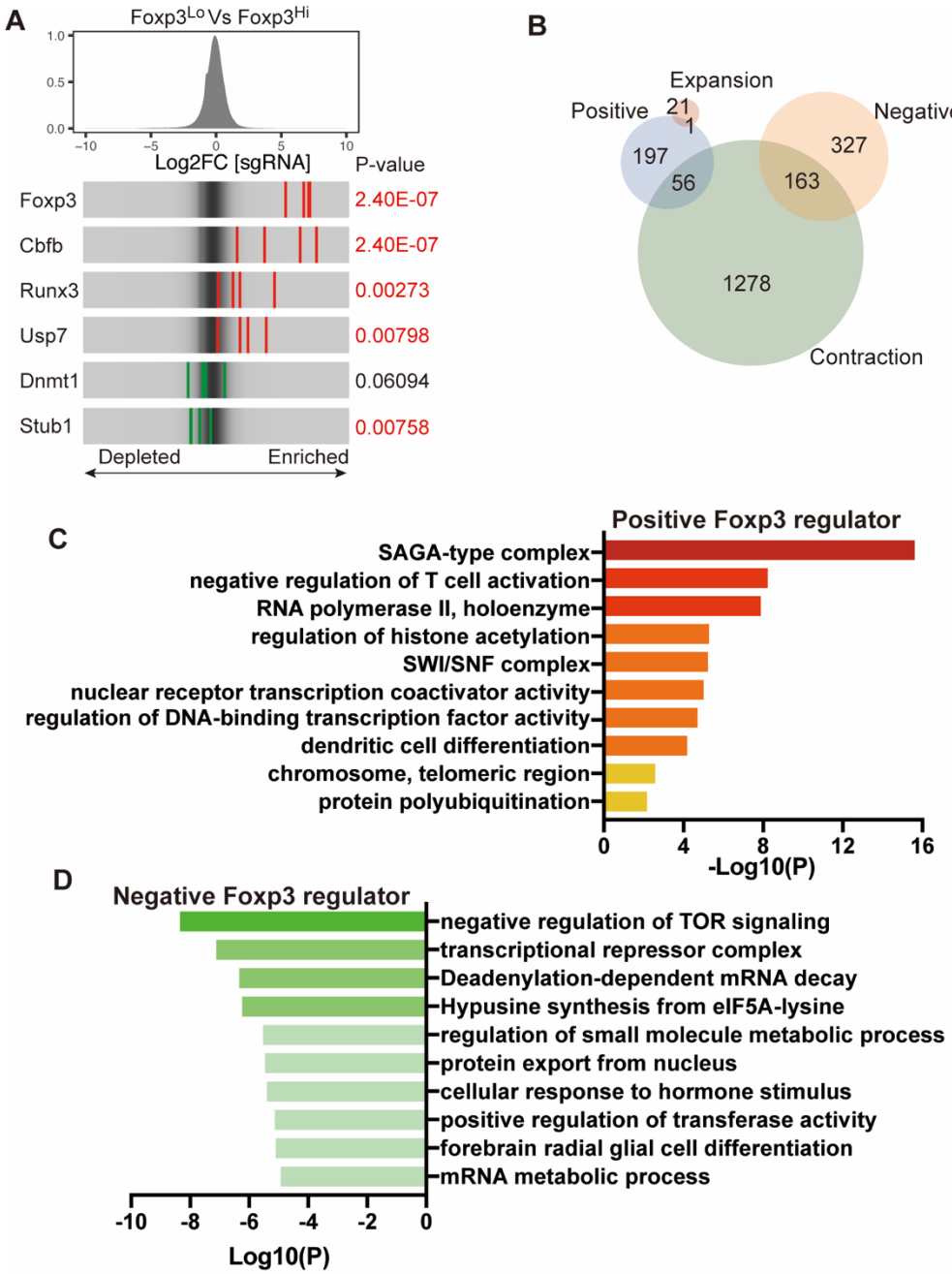

Figure 5. Comparative and gene ontology analyses of Foxp3 regulators

A, Distribution of sgRNA Log2FC comparing Foxp3lo to Foxp3hi. Red stripes represent sgRNAs from positive Foxp3 regulators, whereas green stripes represent sgRNAs from negative Foxp3 regulators. **B,** Venn diagram showing the overlap of Foxp3 regulators with genes involved in cell contraction or expansion. **C, D,** Gene ontology analysis of positive Foxp3 regulators (**C,** 197 genes) **(C)** and negative Foxp3 regulators (**D,** 327 genes) **(D)**. Genes that were not affected cell proliferation were selected for the analysis.

2.2 Validation of the SAGA Complex as a Regulator of Foxp3 Expression and Treg Suppressor Activity

The SAGA complex possesses histone acetyltransferase (HAT) and histone deubiquitinase (DUB) activity, and functions as a transcriptional co-activator through interactions with transcription factors and the general transcriptional machinery(Helmlinger and Tora, 2017; Koutelou et al., 2010). We identified *Ccdc101*, *Tada2b*, and *Tada3* in the HAT module, *Usp22* in the DUB module, and *Tada1*, *Taf6l*, *Supt5*, and *Supt20* from the core structural module among positive Foxp3 regulators that do not affect cell expansion or contraction (Figure 5B, 6A). We sought to validate the potential regulatory function of SAGA complex subunits by using sgRNAs to target individual subunits in Treg cells and measure Foxp3 expression (Figure 6B, 6C). We found that deletion of every subunit tested resulted in a significant and 19-29% reduction in Foxp3 mean fluorescence intensity (MFI). We then further tested the function of SAGA subunit Usp22 in an in vitro suppression assay, which measures the suppression of T cell proliferation when conventional T cells are co-cultured with Treg cells at increasing ratios. We found that Treg cells transduced with sgRNAs targeting *Usp22* had compromised Treg suppressor activity compared with Treg cells transduced with a non-targeting control sgRNA, with significantly more proliferation of T effector cells (Teff) at every ratio of Treg to Teff ratio tested (Figure 6D). These results provide independent validation of our genome-wide screen analyses for this class of chromatin regulators and demonstrate that disrupting the SAGA complex by sgUsp22 reduces Foxp3 expression and Treg suppressor function.

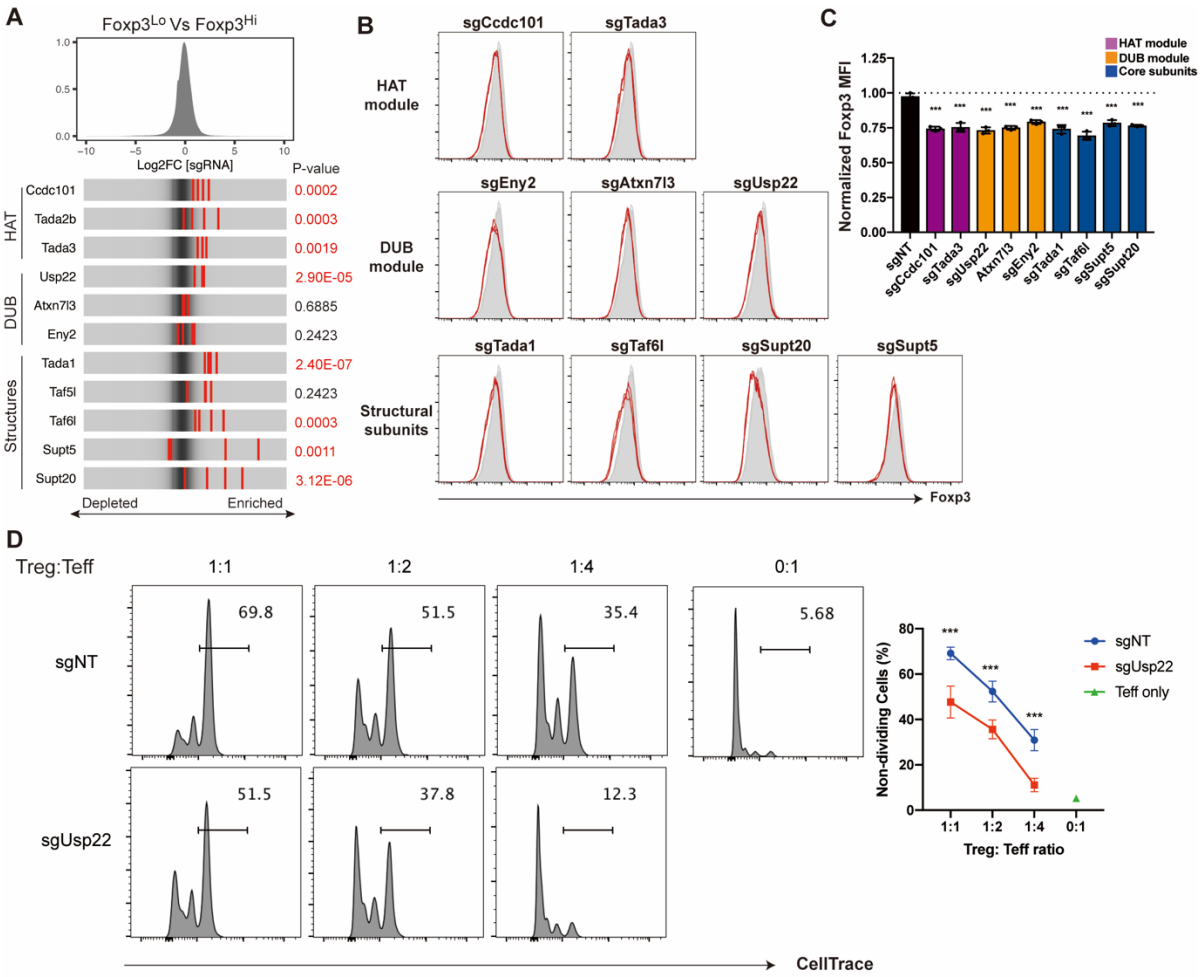

Figure 6. The SAGA complex regulates Foxp3 expression and Treg suppressor activity.

A, Distribution of sgRNA Log2FC comparing Foxp3^{Lo} to Foxp3^{Hi}. Red stripes represent sgRNAs from positive Foxp3 regulators. Genes with a P-value of less than 0.01 are shown in red. **B,** FACS plot of Foxp3 expression in Treg cells transduced with sgRNAs against Ccdc101, Tada3, (HAT module), Eny2, Atxn7l3 and Usp22 (DUB module), and Tada1, Taf6l, Supt20, Supt5 (structural subunits) of SAGA complex (n=3 per group.). **C,** Mean fluorescent intensity (MFI) of Foxp3 in Treg cells transduced with sgRNAs against SAGA subunits. **D,** In vitro suppression assay of Treg cells transduced with sgUsp22. sgNT is non-targeting control. n=3 per group. Data represent mean ± s.d. Statistical analyses were performed using unpaired two-tailed Student's t test (***p<0.001).

2.3 Identification of the Brd9-containing ncBAF Complex as a Specific Regulator of Foxp3 Expression

We next wanted to characterize the role of SWI/SNF complex variants (BAF, ncBAF, and PBAF complexes) in Foxp3 expression. Apart from uniquely incorporating Brd9, the ncBAF complex also contains Gltscr1 or the paralog Gltscr1l and lacks BAF- and PBAF-specific subunits Arid1a, Arid1b, Arid2, Smarce1, Smarcb1, Smarcd2, Smarcd3, Dpf1-3, Pbrm1, Brd7, and Phf10 (Figure 7A). The distinct biochemical compositions of these three SWI/SNF complex assemblies suggest functional diversity. However, it is not known which SWI/SNF complex assemblies are expressed in Treg cells and the potential roles of specific SWI/SNF variants in regulating Foxp3 expression and Treg development have not been studied. Therefore, we performed co-immunoprecipitation assays to probe the composition of SWI/SNF-related complexes in Treg cells. As expected, immunoprecipitation of Smarca4, a core component of all three SWI/SNF complexes, revealed association of common subunits Smarcc1 and Smarcb1, as well as specific subunits Arid1a, Brd9, and Pbrm1. Immunoprecipitations against Arid1a, Brd9, and Phf10 revealed the specific association of these subunits with BAF, ncBAF, and PBAF complexes, respectively (Figure 7B). These results established that all three SWI/SNF complexes are present with the expected composition in Treg cells.

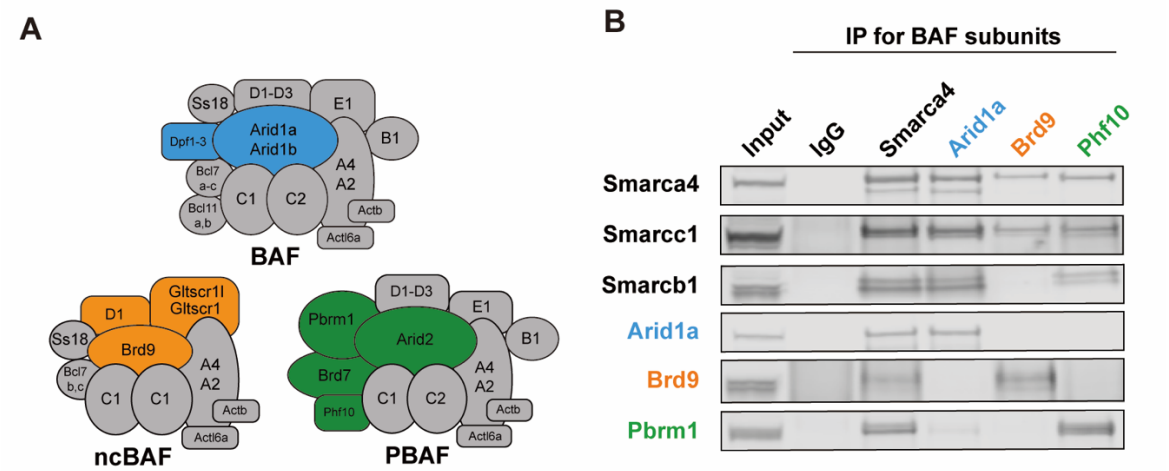

Figure 7. The three SWI/SNF nucleosome remodeling complexes in Treg.

A, A diagram showing three different variants of SWI/SNF complexes: BAF, ncBAF, and PBAF. BAF-specific subunits (Arid1a, Dpf1-3) are colored blue, ncBAF-specific subunits (Brd9, Smarcd1, Gltscr1l, Gltscr1) colored orange, and PBAF-specific subunit (Pbrm1, Arid2, Brd7, Phf10) colored green. Shared components among complexes are colored gray. **B,** Immunoprecipitation assay of Arid1a, Brd9, and Phf10, and Smarca4 in Treg cells. The co-precipitated proteins were probed for shared subunits (Smarca4, Smarcc1, Smarcb1), BAF-specific Arid1a, ncBAF-specific Brd9, and PBAF-specific Pbrm1.

In our screen, we identified *Brd9*, *Smarcd1,* and *Arid1a* among positive regulators of Foxp3, whereas SWI/SNF shared subunits *Smarca4*, *Smarcb1*, *Smarce1*, and *Actl6a* were identified in cell contraction (Supplemental Table 3). This suggests a potential regulatory role for ncBAF and/or BAF complexes. To explore the specific function of BAF, ncBAF, and PBAF complexes in Foxp3 expression, we cloned independent sgRNAs to target unique subunits for each complex, and measured Foxp3 MFI in sgRNA transduced Treg cells. We observed an essential role for the ncBAF complex in Foxp3 expression in Treg cells. Specifically, sgRNA targeting of ncBAF specific subunits, including *Brd9* and *Smarcd1*, significantly diminished Foxp3 expression by nearly 40% in Treg cells (Figure 8A, B, orange). sgRNA targeting of ncBAF-specific paralogs *Gltscr1* and *Gltscr1l* individually resulted in a slight reduction in Foxp3 expression, which was further reduced by *Gltscr1*/*Gltscr1l* double deficiency, suggesting that these two paralogs can compensate in the regulation of Foxp3 expression (Figure 8A, B, orange). In contrast, sgRNA targeting of PBAF specific subunits, including *Pbrm1*, *Arid2*, *Brd7,* and *Phf10*, significantly enhanced Foxp3 expression by as much as 17% (Figure 8A, B, green). sgRNA targeting of BAF specific subunits *Arid1a, Arid1b, Dpf1*, or *Dpf2* did not significantly affect Foxp3 expression (Figure 8A, B, blue). To determine if Arid1a and Arid1b could be compensating for one another, we performed *Arid1a*/*Arid1b* double deletion and found that deletion of either or both Arid paralogs resulted in slight, but non-significant reduction in Foxp3 MFI (Figure 8A, B, blue). These data suggest that ncBAF and PBAF have opposing roles in the regulation of Foxp3 expression. To further explore the role of different SWI/SNF complexes in Treg genome-wide transcription, we performed RNA sequencing from

Treg cells with sgRNA targeting of variant-specific subunits with one or two independent guide RNAs and conducted principal component analysis, which showed that the ncBAF, PBAF, and BAF also have distinct effects at whole transcriptome level in Treg cells (Figure 8C).

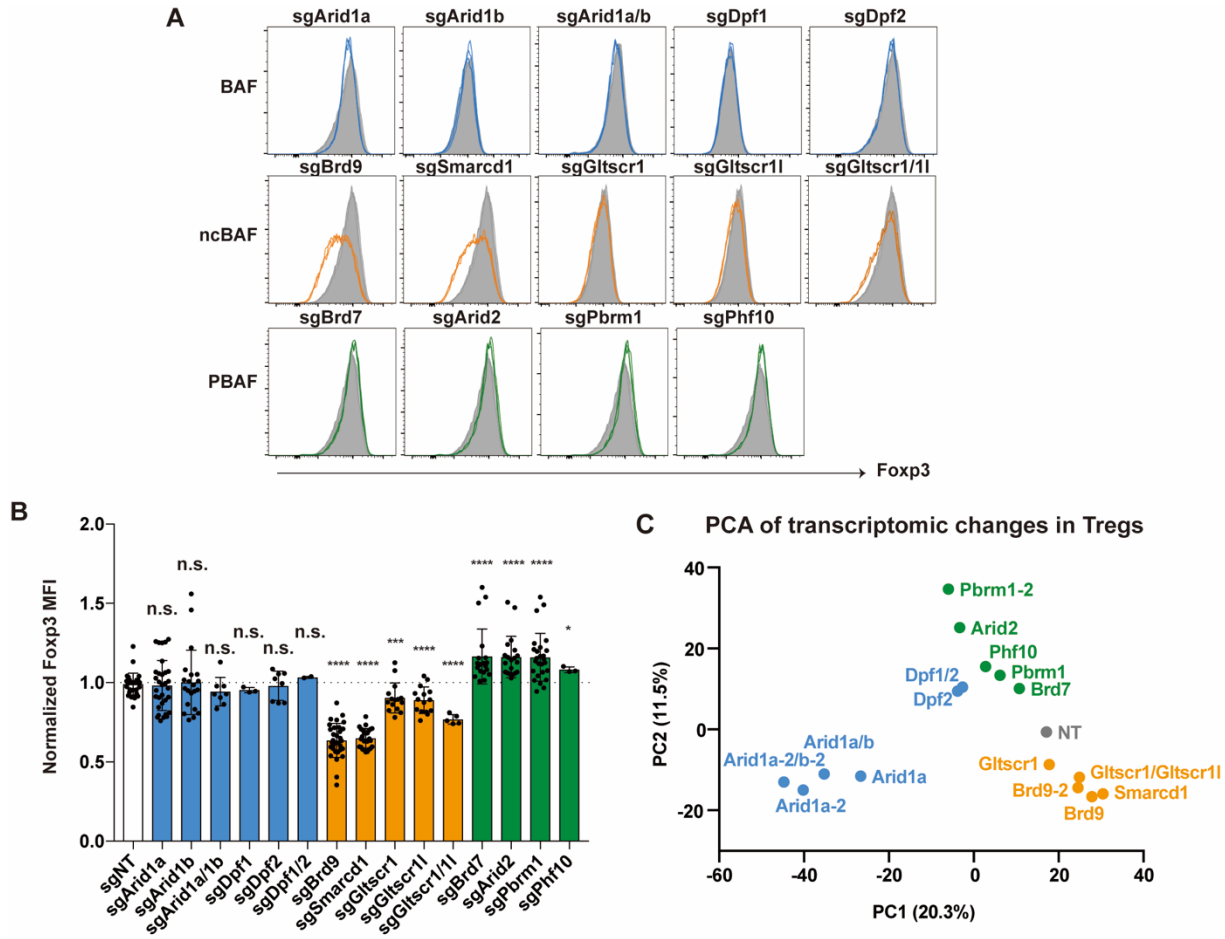

Figure 8. The three SWI/SNF complex assemblies have distinct regulatory roles for Foxp3 expression in Treg.

A, FACS histogram of Foxp3 expression in Treg cells after sgRNA targeting of the indicated SWI/SNF subunits. **B,** Mean fluorescence intensity (MFI) of Foxp3 after sgRNA targeting of the indicated SWI/SNF subunits. Data represents mean and standard deviation of biological replicates (n = 3-21). **C,** Principal component analysis of RNA-seq data collected from Treg cells transduced with guides against the indicated SWI/SNF subunits. In cases where two independent guides were used to target a gene, the second guide for targeting gene indicated as "-2". Data represent mean ± s.d. Statistical analyses were performed using unpaired two-tailed Student's t test (ns: $p \geq 0.05$, *$p < 0.05$, **$p < 0.01$, ***$p < 0.001$, ****$p < 0.0001$).

We then made use of a recently developed chemical Brd9 protein degrader (dBRD9)(Remillard et al., 2017) as an orthogonal method to probe Brd9 function. dBRD9 is a bifunctional molecule that links a small molecule that specifically binds to the bromodomain of Brd9 and another ligand that recruits the cereblon E3 ubiquitin ligase. We confirmed that treatment of Treg cells with dBRD9 resulted in reduced Brd9 protein (Figure 9A). Similar to sgRNA depletion of *Brd9*, dBRD9 treatment significantly decreased Foxp3 expression in Treg cells in a concentration-dependent manner, without affecting cell viability or proliferation (Figure 9B). These data demonstrate the requirement for Brd9 in maintenance of Foxp3 expression using both genetic and chemically-induced proteolysis methods.

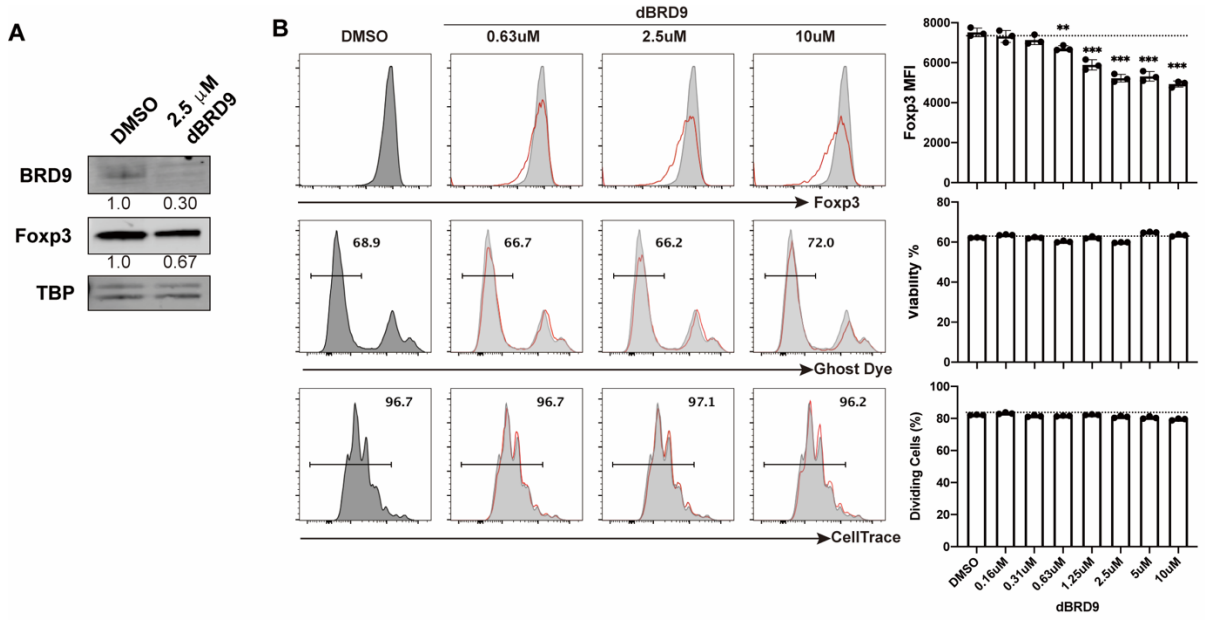

Figure 9. BRD9 degrader dBRD9 reduces Foxp3 expression without affecting cell viability and proliferation.

A, Immunoblotting analysis of BRD9, Foxp3, and TATA-binding protein (TBP) in nuclear lysates from DMSO and 2.5 μM dBRD9 treated Tregs. Normalized protein levels are indicated. **B,** Foxp3 expression, cell viability labeled by Ghost Dye, and cell division determined by CellTrace dilution in Tregs after treatment of dBRD9 in increasing concentrations for 4 days (n=3 per group). Grey shade: DMSO. Red line: dBRD9. Data represents mean ± sd. Statistical analyses were performed using unpaired two-tailed Student's t-test. (*p<0.05, **p<0.01, ***p<0.001).

2.4 Brd9 Regulates Foxp3 Binding at the CNS0 and CNS2 Enhancers and a Subset of Foxp3 Target Sites

To dissect the molecular mechanism of how ncBAF and PBAF complexes regulate Foxp3 expression in Treg cells, we performed chromatin immunoprecipitation followed by genome-wide sequencing (ChIP-seq) in Treg cells using antibodies against the ncBAF-specific subunit Brd9, the PBAF-specific subunit Phf10 and the shared enzymatic subunit Smarca4. Data generated from these ChIP-seq experiments revealed that Brd9, Smarca4, and Phf10 co-localize at CNS2 in the *Foxp3* gene locus and at CNS0 found within the *Ppp1r3f* gene immediately upstream of *Foxp3* (Figure 10A). Since CNS2 was previously shown to regulate stable Foxp3 expression through a positive feedback loop involving Foxp3 binding(Feng et al., 2014; Li et al., 2014b), and Foxp3 is additionally bound at CNS0 in Treg cells (Kitagawa et al., 2017), we rationalized that ncBAF and/or PBAF complexes might affect Foxp3 expression by regulating Foxp3 binding at CNS2/CNS0. We therefore performed Foxp3 ChIP-seq in Treg cells transduced with sgNT, sgFoxp3, sgBrd9 or sgPbrm1. We observed a dramatic reduction in Foxp3 binding at CNS2/CNS0 in sgFoxp3 transduced cells, as expected, and there was also marked reduction of Foxp3 binding at CNS2/CNS0 in *Brd9*-depleted Treg cells (Figure 10A). In contrast, we observed a subtle increase in Foxp3 binding at CNS2/CNS0 in *Pbrm1* sgRNA transduced Treg cells, which could explain why *Pbrm1* emerged as a negative regulator of Foxp3 expression in our validation studies (Figure 10A). These data suggest that Brd9 positively regulates Foxp3 expression by promoting Foxp3 binding to its own enhancers.

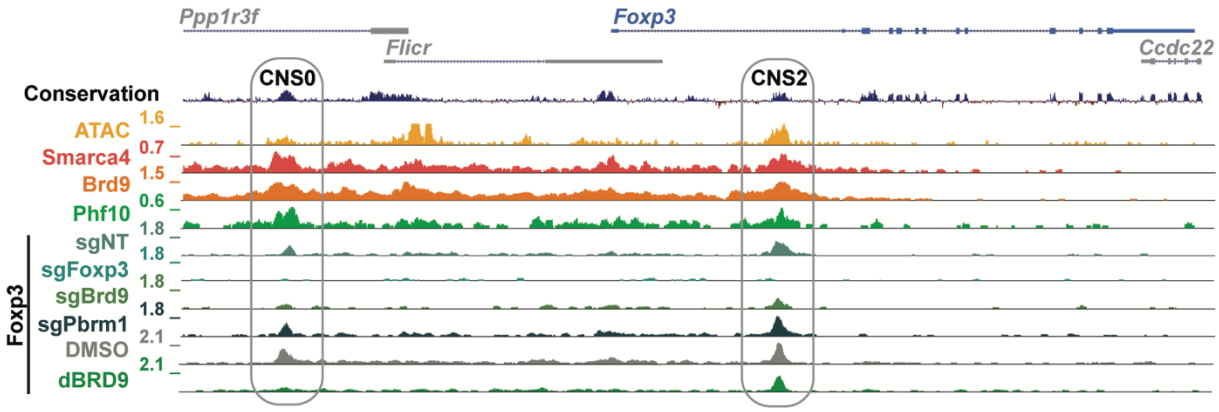

Figure 10. The binding sites of ncBAF, PBAF, and Foxp3 in Foxp3 genomic locus.

Genome browser tracks of Smarca4, Brd9, Phf10 ChIP-seq and ATAC-seq signal, as well as Foxp3 ChIP-seq in sgNT, sgFoxp3, sgBrd9 and sgPbrm1 Treg cells and Foxp3 in DMSO and dBRD9 treated Treg cells (2.5 μM dBRD9 for 4 days). Foxp3 locus is shown with CNS0 and CNS2 enhancers indicated in gray ovals.

We then extended this analysis to examine the cooperation between Brd9 and Foxp3 genome-wide. Notably, we found co-binding of Brd9, Smarca4, and Phf10 with Foxp3 at a subset of Foxp3-bound sites (Figure 11A, B). All four factors localized to promoters, intronic, and intergenic regions of the genome and their binding correlated well with chromatin accessibility as measured by assay of transposase-accessible chromatin with sequencing (ATAC-seq) (Figure 11A, C). Motif analysis of Foxp3-bound sites revealed an enrichment for motifs recognized by Ets and Runx transcription factors consistent with what has been previously shown(Samstein et al., 2012) (Figure 11D). Ets and Runx motifs were also among the most significant motifs at both Brd9-bound sites, along with an enrichment of the Ctcf motif as we and others previously reported(Gatchalian et al., 2018; Michel et al., 2018) (Figure 11E). These results demonstrate that ncBAF and PBAF complexes are co-localized with Foxp3 at Foxp3 binding sites genome-wide.

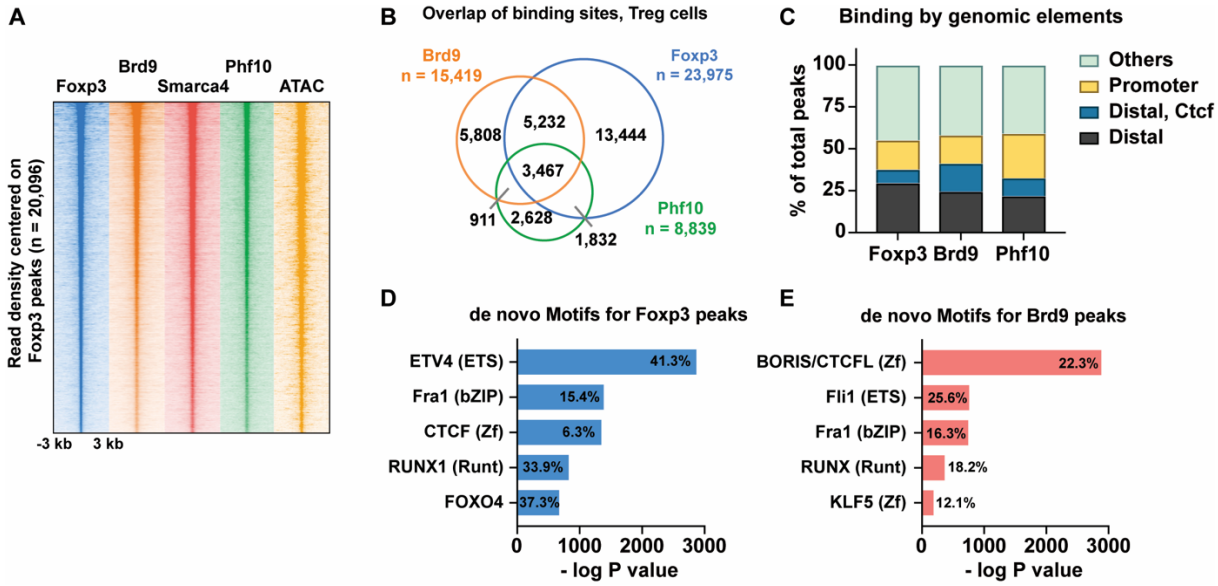

Figure 11. Genome-wide binding sites of ncBAF, PABF, and Foxp3.

A, Heat map of Foxp3, Brd9, Smarca4, Phf10 ChIP-seq and ATAC-seq signal ± 3 kb centered on Foxp3-bound sites in Treg, ranked according to Foxp3 read density. **B,** Venn diagram of the overlap between ChIP-seq peaks in Treg for Brd9, Foxp3, and Phf10 (hypergeometric p value of Brd9:Foxp3 overlap = e^{-27665}, hypergeometric p value of PHF10:Foxp3 overlap = e^{-17185}, hypergeometric p value of Brd9:PHF10 overlap = e^{-14217}). **C,** Stacked bar graph of sites bound by Foxp3, Brd9, and Phf10 that localize to the indicated genomic elements. **D, E,** Bar graph showing the top five de novo motifs enriched at Foxp3 (D), and Brd9 (E) ChIP-seq peaks, the percentage of sites that contain the motif, and negative log of P value (Binomial distribution against random genomic background).

To assess the requirement for Brd9 or Pbrm1 in Foxp3 targeting genome-wide, we analyzed Foxp3 binding in Treg cells transduced with sgNT, sgFoxp3, sgBrd9, or sgPbrm1 at all Foxp3 binding sites (Figure 10, 12A). As expected, we found that Foxp3 binding was lost at over 85% of its binding sites in sgFoxp3-transduced Treg cells (Figure 12B). Foxp3 binding at a subset of these sites was also significantly reduced in sgBrd9-transduced Treg cells (FC 1.5, Poisson $p < 0.0001$) (Figure 12B, C). This was a specific function of Brd9, as Foxp3 binding did not change in *Pbrm1*-depleted Treg cells at these Brd9-dependent sites (Figure 12C). ChIP-seq for the active histone mark H3 lysine27 acetylation (H3K27ac) revealed that Brd9 and Foxp3 cooperate to maintain H3K27ac at over 1,800 shared sites (Figure 12D). At Brd9-dependent Foxp3 sites, for example, we observed a reduction in H3K27ac in sgFoxp3 and sgBrd9-transduced Treg cells, but not in sgPbrm1-transduced Treg cells (Figure 12E). Using dBRD9, we further recapitulated our observation that Brd9 loss resulted in diminished Foxp3 binding to chromatin at a subset of Foxp3 target sites (Figure 12F-H), including at CNS2 and CNS0 (Figure 10). To determine if ncBAF complexes maintain chromatin accessibility for Foxp3 binding, we performed ATAC-seq on sgBrd9 and sgNT Treg cells (Figure 12I). Only 61/1699 (3.5%) of Brd9-dependent Foxp3 binding sites had a significant reduction in chromatin accessibility in sgBrd9 Treg cells, suggesting that chromatin remodeling may only minimally contribute to ncBAF-dependent maintenance of Foxp3 binding.

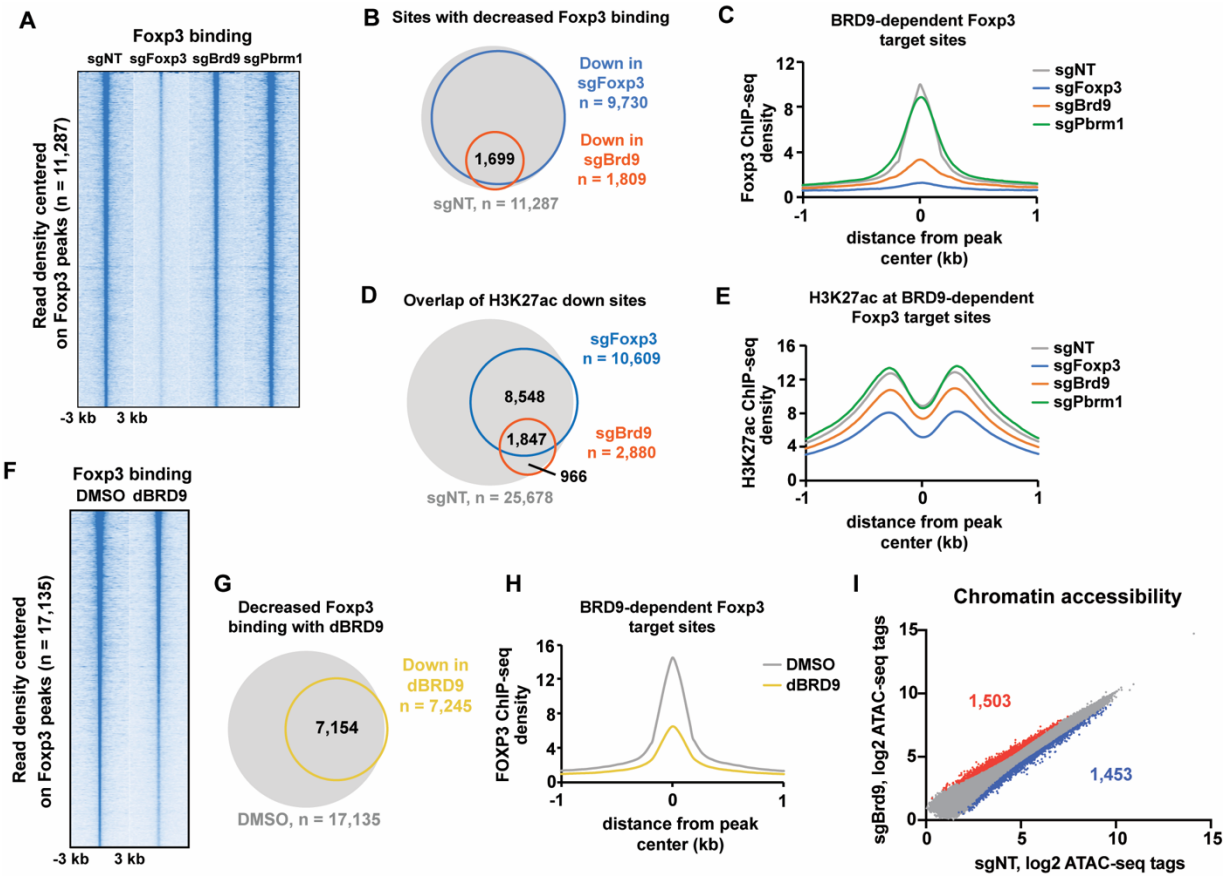

Figure 12. Functional genomic analyses of Treg in the absence of ncBAF.

A, Heat map of Foxp3 ChIP-seq signal in sgNT, sgFoxp3, sgBrd9 and sgPbrm1 Treg cells ± 3 kilobases (kb) centered on Foxp3-bound sites in sgNT, ranked according to read density. **B,** Venn diagram of the overlap (hypergeometric p value = $e^{-11,653}$) between sites that significantly lose Foxp3 binding (FC 1.5, Poisson p value < 0.0001) in sgFoxp3 and sgBrd9, overlaid on all Foxp3-bound sites in sgNT (in gray). **C,** Histogram of Foxp3 ChIP read density ± 1 kb surrounding the peak center of sites that significantly lose Foxp3 binding in both sgFoxp3 and sgBrd9 (n=1,699) in sgNT, sgFoxp3, sgBrd9 and sgPbrm1. **D,** As in B, but for sites that lose H3K27ac (FC 1.5, Poisson p value < 0.0001, hypergeometric p value of overlap = $e^{-7,938}$). **E,** As in C, but for H3K27ac ChIP read density. **F,** As in A, but for Foxp3 ChIP-seq signal in DMSO- and dBRD9 treated Treg cells at all Foxp3-bound sites in DMSO. **G,** As in B, but for sites that significantly lose Foxp3 binding in dBRD9 treated Treg cells versus DMSO (FC 1.5, Poisson p value < 0.0001). **H,** As in C, but for DMSO and dBRD9 treated cells. **I,** Scatterplot of Log2 ATAC-seq mean tags of duplicates in sgNT versus sgBrd9 Treg cells.

Since Brd9 deficiency leads to reduced Foxp3 expression, we next asked the question whether reduced Foxp3 binding to its target regions in sgBrd9 Treg cells is due to reduced Foxp3 protein, or Brd9 plays an additional role in facilitating Foxp3 binding to a subset of its targets. To this end, we ectopically expressed Foxp3 or MIGR vector control in sgNT and sgBrd9 transduced Treg cells, and performed Foxp3 ChIP-seq in these cells. Analysis of the Foxp3 ChIP-seq result showed that ectopic Foxp3 expression partially restored Foxp3 binding in sgBrd9 Treg cells, but not to the level of sgNT alone or sgNT with ectopic Foxp3 expression (Figure 13A). Further analysis revealed that while ectopic Foxp3 expression restored Foxp3 binding to a portion of Brd9-dependent Foxp3 binding sites (e.g. *CD44* intergenic, *Tigit* intergenic, and *Ctla2a* promoter), binding to the majority of Brd9-dependent sites (~71%) (e.g. *Icos* intergenic, *Ctla4* intergenic, and *Ctla4* promoter) was not rescued by simply restoring Foxp3 expression (Figure 13B, C). These data demonstrate that Brd9 co-binds with Foxp3 at the *Foxp3* locus to positively reinforce its expression. Brd9 additionally promotes Foxp3 binding and H3K27ac at a subset of Foxp3 target sites both by potentiating Foxp3 expression and through epigenetic regulation at Brd9/Foxp3 co-bound sites.

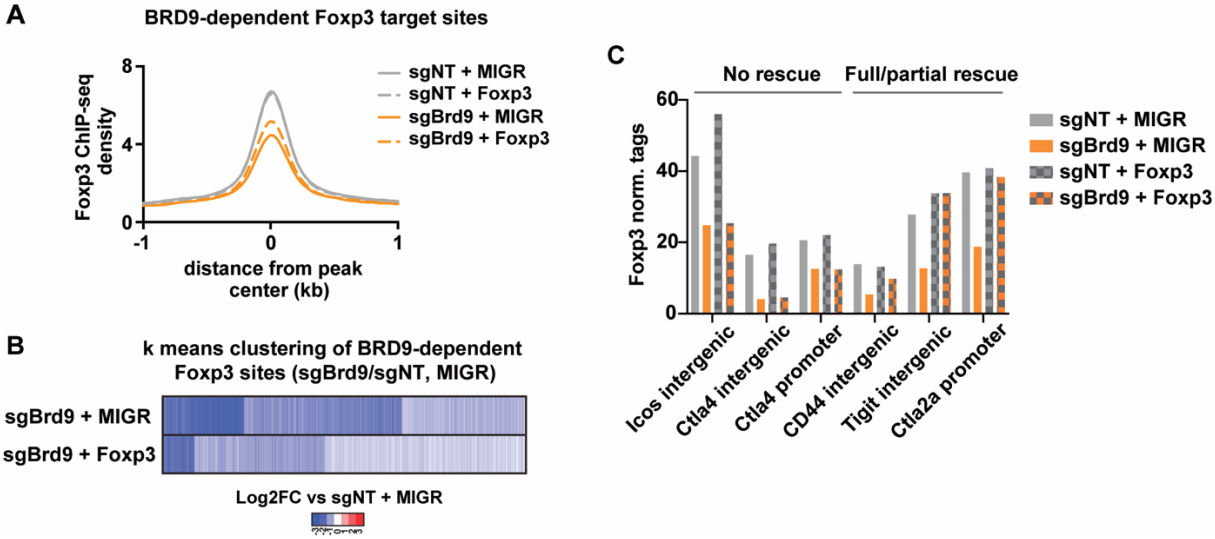

Figure 13. Over-expressed Foxp3 partially rescues Foxp3 binding in Brd9-deficient Treg.

A, Histogram of Foxp3 ChIP read density ± 1 kb surrounding the peak center of sites that significantly lose Foxp3 binding Treg cells transduced with either sgNT or sgBrd9, with ectopic expression of either MIGR vector control or Foxp3. **B,** Heatmap of k-means clusters based on Log2FC Foxp3 ChIP-seq signal in sgBrd9+MIGR vs sgNT+MIGR. **C,** Bar graph showing Foxp3 ChIP-seq signal at select genomic regions.

2.5 Brd9 Co-regulates the Expression of Foxp3 and a Subset of Foxp3 Target Genes

Based on co-binding of Brd9 and Foxp3 at Foxp3 target sites, we assessed the effects of Brd9 ablation on the transcription of Foxp3 target genes. We performed RNA-seq in Treg cells transduced with sgFoxp3, sgBrd9, or sgNT. Consistent with Foxp3's role as both transcriptional activator and repressor, we observed 793 genes with reduced expression and 532 genes with increased expression in *Foxp3* sgRNA transduced Treg cells, which are enriched in 'cytokine production', 'regulation of defense response', and 'regulation of cell adhesion' (Figure 14A, B). Of these, 72% were directly bound by Foxp3 in our ChIP-seq dataset and 56% were co-bound by Foxp3 and Brd9 (Figure 14C). Based on this co-binding, we next examined whether Brd9 regulates Foxp3 target gene expression through positively affecting Foxp3 binding to its targets. Gene set enrichment analysis (GSEA) demonstrated that the sgBrd9 increased genes are significantly enriched among genes that increase upon sgFoxp3 targeting, while the sgBrd9 decreased genes are enriched among genes that decrease in sgFoxp3 Treg cells (Figure 14D). We also performed RNA-seq for Treg cells treated with either vehicle or the dBRD9 degrader and observed a similar significant enrichment for dBRD9 affected genes among the Foxp3 regulated genes (Figure 14E). To determine how Brd9 control of Foxp3 binding affects gene expression, we divided Foxp3 binding sites into quartiles based on most affected (Brd9-dependent) to least affected (Brd9-independent) by sgBrd9 transduction and compared fold changes in gene expression in sgBrd9 versus sgNT Treg cells. Indeed, gene expression of Brd9-dependent Foxp3 target genes was significantly more affected upon sgBrd9 targeting

than expression of Brd9-independent Foxp3 target genes (Figure 14F). Furthermore, gene expression was significantly more affected in sgSmarcd1 transduced (an ncBAF subunit) Treg cells, but not in sgPbrm1 transduced (a PBAF subunit) Treg cells, at Brd9-dependent Foxp3 target genes (Figure 14F). Thus, ncBAF complexes regulate Foxp3 target genes through potentiation of Foxp3 binding at its target sites. Notably, the Brd9-dependent target gene sets generated from our RNA-seq data were among the most significantly enriched dataset of 9,229 immunological, gene ontology and curated gene sets when analyzed against the sgFoxp3 transduced Treg expression data (Figure 14G). In addition, both datasets were significantly enriched for genes that are differentially expressed between Treg and conventional T cell (Feuerer et al., 2010), and between Foxp3 mutant Treg from *scurfy* mice and wild-type Treg (Hill et al., 2007). These data define a role for Brd9 in Treg through specifically regulating the expression of Foxp3 itself and a subset of Foxp3 target genes.

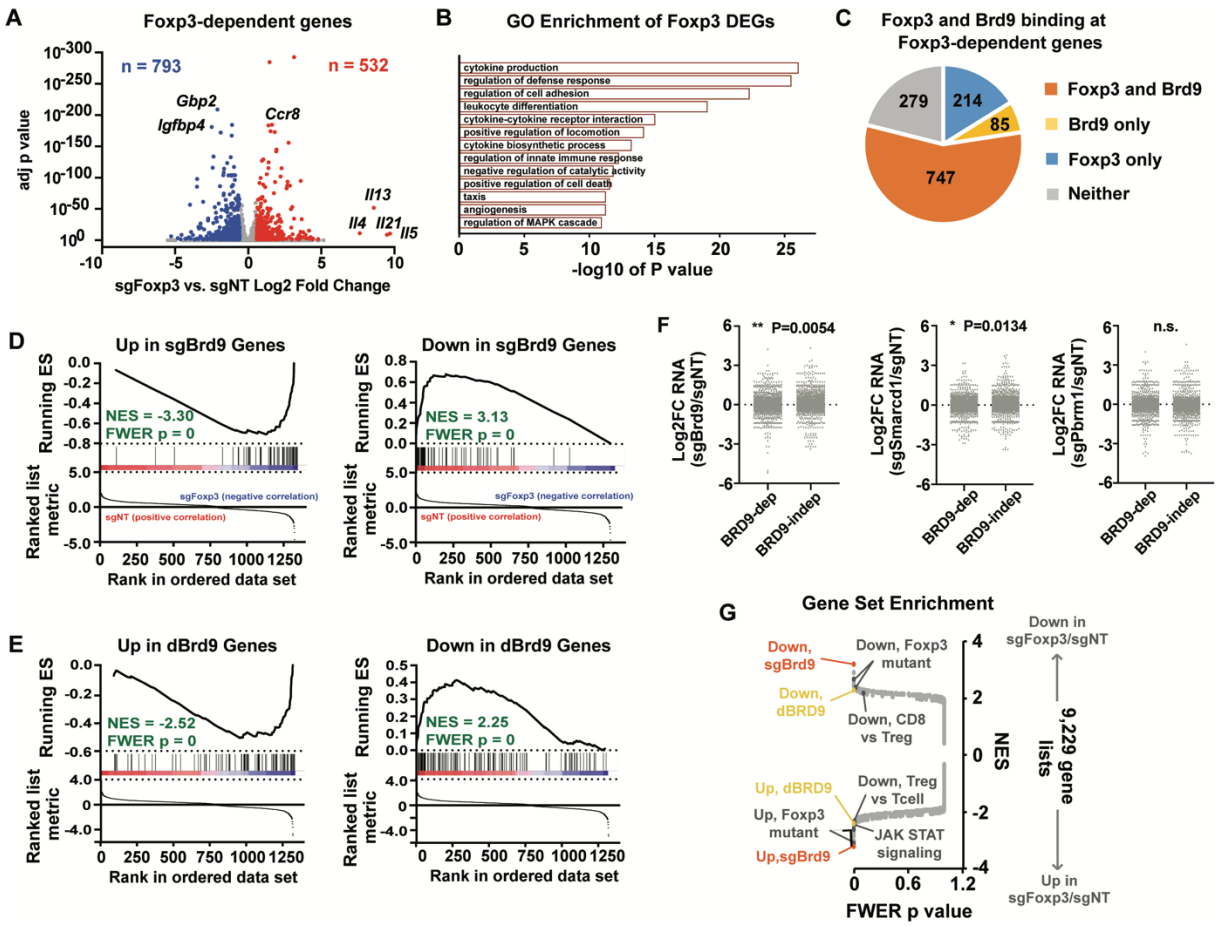

Figure 14. Brd9 co-regulates the expression of Foxp3 and a subset of Foxp3 target genes.

A, Volcano plot of log2 fold change RNA expression in sgFoxp3/sgNT Treg cells versus adjusted p value (Benjamin-Hochberg). Number of down and up genes are indicated, which are colored blue and red, respectively. **B,** Significance of enrichment of Foxp3-dependent genes in each gene ontology. **C,** Pie chart of Foxp3 and Brd9 binding by ChIP-seq for Foxp3-dependent genes. **D,** Gene set enrichment analysis (GSEA) enrichment plot for up and down genes in sgBrd9/sgNT compared with RNA-seq data of genes that significantly change in sgFoxp3/sgNT Treg cells. ES: Enrichment Score, NES: Normalized Enrichment Score, FWER: Familywise Error Rate. **E**, As in **D**, but for up and down genes in dBRD9/DMSO Treg cells. **F,** Log2FC RNA in sgBrd9/sgNT, sgSmarcd1/sgNT, and sgPbrm1/ sgNT of genes that are annotated to sites that are most and least affected by Brd9-dependent Foxp3 change in binding. See Methods section for details of analysis. Unpaired two-tailed Student's t test. **G,** GSEA of the sgFoxp3/sgNT RNA-seq data; plot shows the familywise error rate (FWER) p value versus the normalized enrichment score (NES). See also Supplemental Table 5.

2.6 The ncBAF Complex is Required for Normal Treg Cell Suppressor Activity *In Vitro* and *In Vivo*.

The divergent roles of ncBAF and PBAF complexes in regulating Foxp3 expression suggested that these complexes might also differentially affect Treg suppressor function. We performed sgRNA targeting of ncBAF-specific *Brd9* and *Smarcd1* or PBAF-specific *Pbrm1* and *Phf10* in Treg cells and measured their function by conducting an *in vitro* suppression assay. Treg cells depleted of *Brd9* or *Smarcd1* exhibited significantly reduced suppressor function, whereas depletion of *Pbrm1* or *Phf10* resulted in significantly enhanced suppressor function (Figure 15A). These data demonstrate that the opposing regulation of Foxp3 expression by ncBAF and PBAF complexes results in decreased/increased Treg suppressor activity upon ncBAF or PBAF subunit deletion, respectively. Similar to sgRNA depletion of *Brd9*, Treg cells treated with dBRD9 also showed significantly and specifically compromised Treg suppressor function *in vitro* (Figure 15B). We next determined if the reduced suppressor activity in sgBrd9 Treg cells could be rescued by overexpression of Foxp3. We found that ectopic expression of Foxp3 in sgBrd9 Treg cells partially restored Treg suppressor activity to a level comparable to sgNT controls, but still lower compared to sgNT Treg cells with ectopic Foxp3 expression (Figure 16A, B). These results underscore the requirement for Brd9 in Foxp3 expression maintenance and optimal Treg suppressor activity, and further demonstrate that dBRD9 reduces Treg suppressor activity without impairing T effector responses *in vitro*.

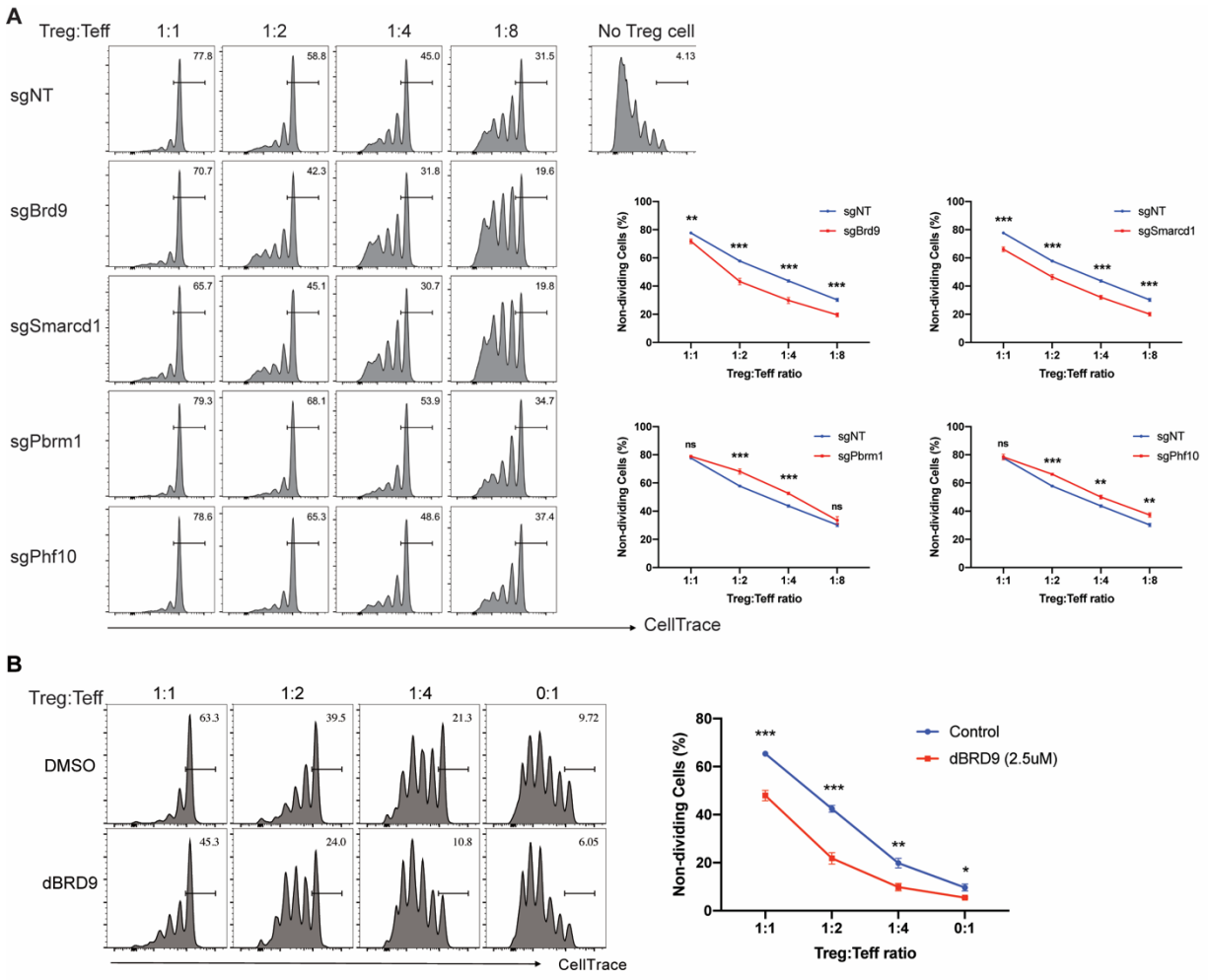

Figure 15. The ncBAF complex regulates Treg suppressor function *in vitro.*

A. *In vitro* suppression assay of Treg cells with sgRNA targeting of *Brd9, Smarcd1, Pbrm1,* and *Phf10.* sgNT was used as non-targeting control. Representative histograms (left) of effector T cell divisions in different Treg:Teff ratios. (n=3 per group, data represent ± s.d.). **B**, *In vitro* suppression assay using Treg cells treated with dBRD9 or vehicle DMSO. Representative histograms (left) of effector T cell divisions in different Treg:Teff ratios. (n=3 per group, data represent ± s.d.). Statistical analyses were performed using unpaired two-tailed Student's t test (ns: $p \geq 0.05$, *$p<0.05$, **$p<0.01$, ***$p<0.001$).

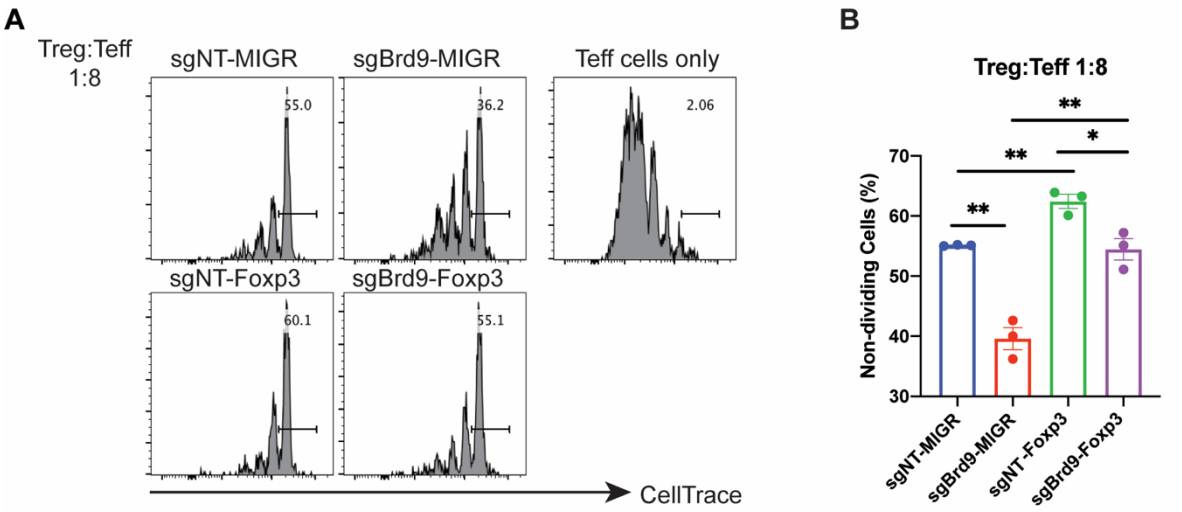

Figure 16. Overexpressed Foxp3 partially fully rescues Brd9-deficient Treg suppressor function *in vitro*.

In vitro suppression assay of sgBrd9 or sgNT with ectopic expression of Foxp3 or control vector MIGR1. Representative histogram **(A)** and bar graph **(B)** of effector T cells divisions in Treg:Teff mixed in 1:8 ratio. (n=3 per group, data represent ± s.d.). Statistical analyses were performed using unpaired two-tailed Student's t test (ns: $p \geq 0.05$, *$p < 0.05$, **$p < 0.01$).

To test if Brd9 also affects Treg function *in vivo*, we utilized a T cell transfer-induced colitis model. In this model, *Rag1*$^{-/-}$ mice were either transferred with CD45.1^{+} CD4^{+} CD25^{-}CD45RB^{hi} effector T cell (Teff) only, or co-transferred with Teff along with CD45.2^{+} Treg cells transduced with sgBrd9 or control sgNT (Figure 17A). Mice transferred with Teff cells alone lost body weight progressively due to development of colitis. Co-transfer of Treg cells transduced with sgNT protected recipient mice from weight loss, whereas co-transfer of sgBrd9 transduced Treg cells failed to protect recipients from losing weight (Figure 17B). The mice transferred with *Brd9*-depleted Treg cells showed significant colitis pathology at seven weeks compared to mice that received control Treg cells (Figure 17C). Furthermore, *Brd9* depletion also led to compromised Treg stability after transfer, manifested by reduced Foxp3^{+} cell frequencies within the CD45.2^{+}CD4^{+} transferred Treg population (Figure 17D). These results demonstrate that Brd9 is an essential regulator of normal Foxp3 expression and Treg function in a model of inflammatory bowel disease *in vivo*.

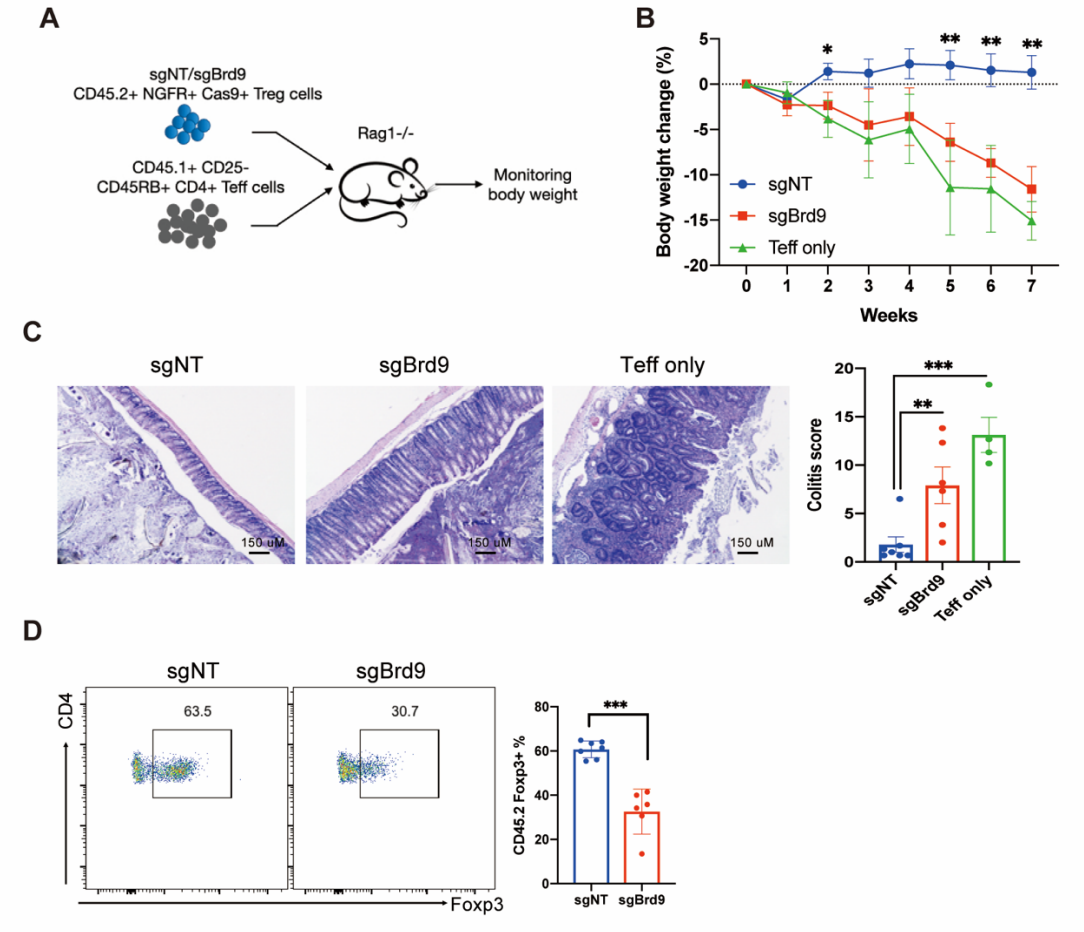

Figure 17. The ncBAF complex regulates Treg suppressor function *in vivo*.

Experiment to measure Treg function of sgNT or sgBrd9 Treg cells relative to no Treg cells in a T cell transfer induced colitis model. **A,** Experimental procedure. **B,** Body weight loss. **C,** Colon histology (left) and colitis scores (right). **D,** Percentage of Foxp3$^+$ cells in transferred CD45.2$^+$CD4$^+$ Treg population at end point. (n=4-6 per group. Data represent mean ± s.e.m.) Statistical analyses were performed using unpaired two-tailed Student's t test (ns: $p \geq 0.05$, *$p<0.05$, **$p<0.01$, ***$p<0.001$).

In addition to their beneficial role in preventing autoimmune diseases, Treg cells also function as a barrier to anti-tumor immunity. We therefore wondered whether we could exploit the compromised suppressor function shown in *Brd9* deficient Treg to disrupt Treg-mediated immune suppression in tumors. We used the MC38 colorectal tumor cell line to induce cancer due to the prominent role Treg plays in this cancer model(Delgoffe et al., 2013). *Rag1*$^{-/-}$ mice were used as recipients for adoptive transfer of Treg depleted-CD4 and CD8 T cells (Teff) only, or co-transfer of Teff with Treg cells transduced with either sgBrd9 or sgNT. MC38 tumor cells were implanted subcutaneously on the following day (Figure 18A). Transfer of sgNT Treg cells allowed for significantly faster tumor growth compared to mice that received Teff cells only ("No Treg") due to suppression of the anti-tumor immune response by Treg cells (Figure 18B, C). Furthermore, tumor growth in mice that received sgBrd9 transduced Treg cells was significantly slower than in mice that received sgNT Treg cells, consistent with our findings that *Brd9* deficiency reduced Treg suppressor activity (Figure 18B, C). Both CD4 and CD8 T cell tumor infiltration significantly increased in mice that received sgBrd9 transduced Treg cells compared to sgNT Treg cells (Figure 18D, E). Additionally, the percentage of IFN-□ producing intra-tumor CD4 and CD8 T cells in mice that received sgBrd9 transduced Treg cells was significantly greater than the sgNT Treg condition, and comparable to the transfer of Teff alone ("No Treg") (Figure 18F, G). Consistent with our findings that Brd9 is required for Treg persistence *in vivo* (Figure 17C), the percentage of transferred Treg cells was reduced in mice that received sgBrd9 transduced Treg cells relative to sgNT Treg cells (Figure 18H). Overall, a 2-3 fold increase in the ratio of CD8 T cells to Treg cells in tumor and spleen was observed

in the sgBrd9 versus the sgNT condition, consistent with the enhanced anti-tumor immune response in mice that received sgBrd9 transduced Treg cells (Figure 18I). To examine if Brd9 deficiency promotes generation of inflammatory ex-Treg cells, we measured Foxp3 and IFN-□ expression within the transferred sgBrd9 or sgNT Treg population marked with a GFP reporter. Ablation of Brd9 led to an increase in the $GFP^{+}Foxp3^{-}$ ex-Treg population compared to sgNT Treg cells (Figure 18J, L). More importantly, a higher percentage of sgBrd9 ex-Treg cells produced IFN-□ compared to sgNT ex-Treg cells (Figure 18K, L), contributing to slower tumor growth in mice that received sgBrd9 Treg cells. This experiment demonstrates that Brd9 promotes Treg lineage stability and suppressive function in MC38 tumors and *Brd9* deficiency in Treg improves anti-tumor immunity in this context.

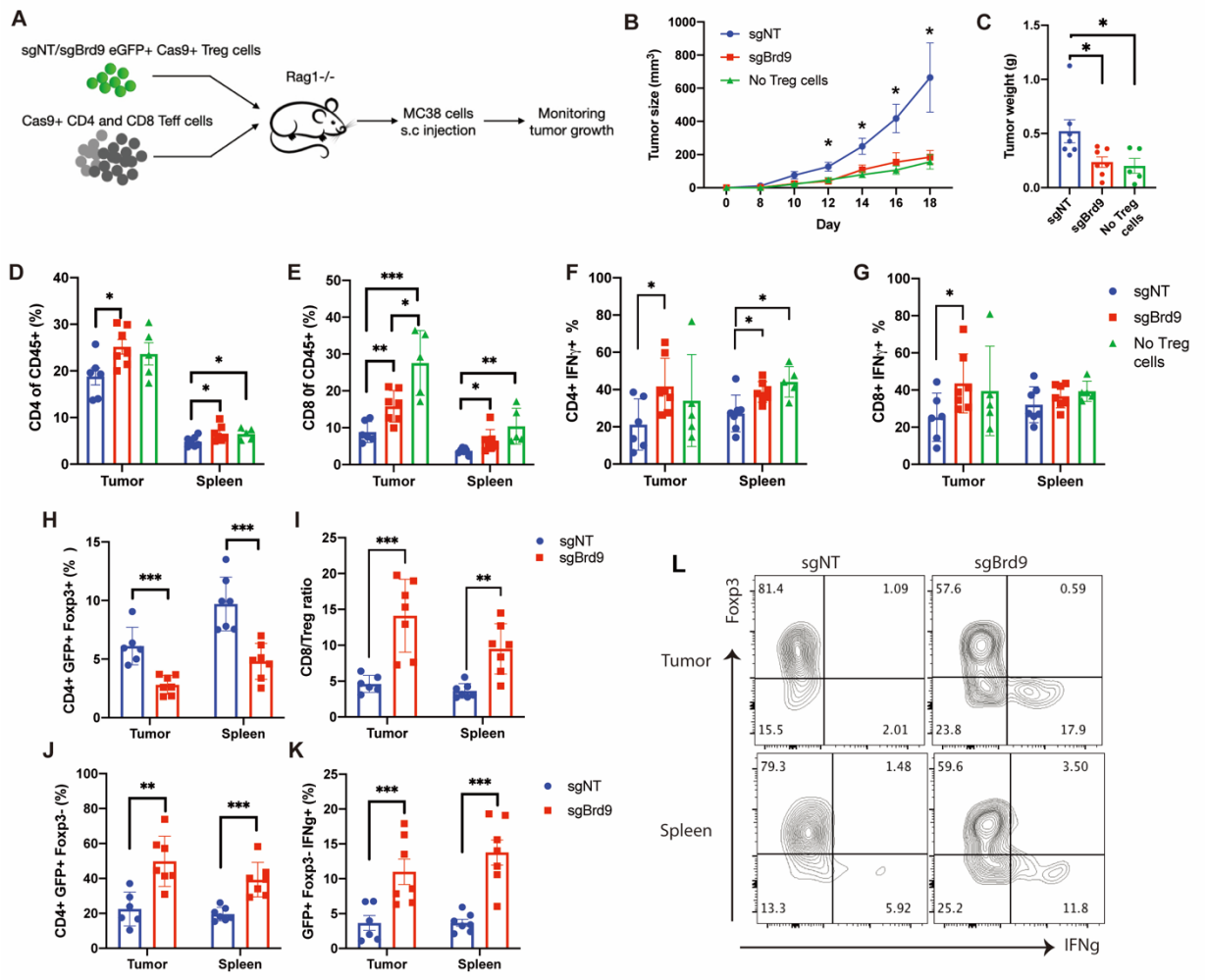

Figure 18. Targeting Brd9 in Treg improves anti-tumor immunity.

A, Experiment procedure to measure function of sgNT or sgBrd9 Treg cells relative to no Treg cells in MC38 tumor model. **B,** Tumor growth curve. **C,** Tumor weight at end point. **D, E,** Bar graph of total CD4 T cells (D) and CD8 T cells (E) percentage in CD45+ immune cell population. **F, G,** Bar graph of IFN-β+ cell percentage in CD4 T cells (F) and in CD8 T cells (G). **H,** Bar graph of CD4+GFP+Foxp3+ donor cell percentage in CD4 T cells. **I,** Ratio of CD8/Treg. **J,** Bar graph of Foxp3- ex-Treg cell percentage in the transferred Treg population marked by the GFP reporter. **K,** Bar graph of Foxp3- IFN- β + cell percentage in the transferred Treg population. **L,** FACS analysis of Foxp3 and IFN- β expression in donor Treg cell population (CD4+ GFP+) in MC38 tumor and spleen at the end point. (n=5-7 per group. Data represent mean ± s.e.m.) Statistical analyses were performed using unpaired two-tailed Student's t test (ns: $p \geq 0.05$, *$p<0.05$, **$p<0.01$, ***$p<0.001$).

CHAPTER THREE: CONCLUDING REMARKS

3.1 Summary of Finding

In this study, we performed a genome-wide CRISPR screen to identify positive and negative regulators of Foxp3 expression in mouse natural Treg. Among positive regulators, we identified *Cbfb and Runx3*, consistent with a requirement for Cbf-ß/Runx3 in Foxp3 expression and Foxp3-dependent target gene expression(Kitoh et al., 2009; Rudra et al., 2009). Among the positive regulators, we discovered subunits from two chromatin remodeling complexes, the Brd9-containing ncBAF and SAGA complexes. Independent validation and functional assays demonstrated an essential role for the ncBAF complex and SAGA complex in Foxp3 expression and Treg suppressor function. A recent study using CRISPR screen of 489 nuclear factors also identified Usp22, a subunit of the SAGA complex, as a positive regulator of Foxp3 expression (Cortez et al., 2020). ncBAF subunits *Brd9, Gltscr1, Gltscr1l,* or *Smarcd1* were not identified in this study due to exclusion of these genes in the sgRNA library.

Our screens also confirmed several known negative regulators of Foxp3, including DNA methyl-transferase *Dnmt1* and the ubiquitin ligase *Stub1*. Additionally, we identified multiple negative regulators of the mTOR pathway as Foxp3 negative regulators (*Tsc2*, *Flcn*, *Ddit4*, *Sesn2*, *Nprl2*), confirming an essential role for mTOR in homeostasis and function of activated Treg (Chapman et al., 2018; Sun et al., 2018). Among negative Foxp3 regulators, we uncovered genes encoding regulators of RNA metabolism, which have no previously reported function in Foxp3 expression. For example, *Mettl3* and *Mettl14* form a methyltransferase complex that is essential for the

m^6A methylation of RNA, which is recognized as an important regulatory mechanism for a wide range of biological processes, including RNA stability, protein translation, stem cell self-renewal, cell lineage determination, and oncogenesis (Yue et al., 2015). Our screen suggests a potentially role for RNA m^6A methylation in post-transcriptional regulation of Foxp3. Together, our genome-wide screen provides the first comprehensive picture of the complex regulatory network controlling Foxp3 expression and reveals previously unknown pathways and factors that warrant further investigation.

Following the identification of SWI/SNF subunit genes among Foxp3 regulators, we endeavored to characterize the roles of the three SWI/SNF-related complexes by deleting subunits unique to each of the ncBAF, BAF, and PBAF complexes. We observed specific and divergent roles of ncBAF and PBAF complexes in regulating Foxp3 expression in Treg. In contrast, deletion of BAF-specific subunits had a slight, but non-significant effect on Foxp3 expression. Nevertheless, several SWI/SNF core subunits were recovered in our screen among genes that regulate Treg cell contraction, suggesting that BAF complexes may regulate Treg cell activation or proliferation in response to TCR stimulation used to activate and culture Treg cell in our screen. This is consistent with the fact that genetic deletion of *Smarca4* in Treg cells results in the development of a fatal inflammatory disorder reminiscent of Foxp3 mutant *scurfy* mice (Chaiyachati et al., 2013). While Treg cell development and Foxp3 expression are normal in *Smarca4* deficient Treg cells, Treg cell function is nevertheless compromised due to impaired activation of TCR target genes, for example chemokine receptor genes (Chaiyachati et al., 2013). Thus, deletion of *Smarca4* or other BAF complex subunits

likely results in overall defects in Treg fitness, whereas deletion of ncBAF subunits appears to have a selective effect on Foxp3 expression and its target genes. Mechanistically, we found that the ncBAF complex co-bound and cooperated with Foxp3 to potentiate its binding to the CNS2 and CNS0 enhancers of the *Foxp3* locus. In addition to the Foxp3 locus itself, our ChIP-seq analysis revealed that ncBAF also colocalized with Foxp3 at regulatory elements in a subset of Foxp3 target genes to regulate their gene expression. Thus, we favor a model in which reduced Foxp3 expression and loss of epigenetic regulation by ncBAF complexes upon sgBrd9 transduction results in less Foxp3 binding at Brd9/Foxp3 co-bound sites, thereby affecting Foxp3 target gene expression.

Finally, we tested the *in vivo* relevance of our findings by disrupting the ncBAF subunit Brd9 in Treg in mouse models of inflammatory bowel disease and cancer. *Brd9* deficiency in Treg cells weakened their suppressor function in a model of T cell induced colitis, leading to exacerbated disease progression. In the context of cancer, we found that transfer of *Brd9* deficient Treg cells failed to restrict anti-tumor immune responses in the MC38 cell induced cancer model, leading to slower tumor growth. Currently, there is a concerted effort to develop compounds targeting a number of SWI/SNF complex subunits to modulate their function. Our data show that bromodomain-directed degradation of Brd9 by dBRD9 recapitulated the effects of *Brd9* genetic deletion, suggesting that the ncBAF complex can be targeted with small molecules to control Foxp3 expression and Treg function. Thus, through the unbiased screen of Foxp3 regulators, we identify proteins that can potentially be targeted to manipulate Treg

homeostasis and function in autoimmune diseases and cancer. Finally, we utilized adoptive transfer of Treg cells into Rag1$^{-/-}$ mice to test the *in vivo* function of sgBrd9 Treg cells in models of colitis and tumor immunity. Although this approach is commonly used, the rapid homeostatic proliferation of Treg cells in recipient mice may impose additional influence on their immune suppressor function, so Treg cell-specific conditional deletion approaches will be necessary to further study the functional relevance of candidates identified in this screen.

3.2 Future Direction

Identification of ncBAF complexes mediates Foxp3 binding and expression raises several questions. First of all, how ncBAF complexes regulate Foxp3 binding? SWI/SNF complexes have been known for their ability to remodel nucleosome. One possibility is that ncBAF complexes maintain chromatin accessibility for Foxp3 binding; however, we detected minimal changes in chromatin accessibility upon sgBrd9 targeting by ATAC-seq. We speculate that alternative methods for mapping nucleosome dynamics and/or chromatin accessibility are necessary to determine the role of chromatin remodeling in this setting. Secondly, given that ncBAF complexes highly localize on the CTCF motif, another possibility is that ncBAF complexes regulate Treg's spatial chromatin structure, thus enforcing optimal expression of Foxp3. Besides, it is unclear how ncBAF complex can be recruited to certain genomic location. The ncBAF may act by recognizing certain histone marks or recruiting by certain transcription factors. Identifying ncBAF interactome by mass spectrometry may reveal the clue. Lastly, our study showed both SWI/SNF and SAGA complexes are required for Foxp3 expression. It is currently

unclear whether these two complexes work together in controlling Foxp3 expression; therefore it is interesting to characterize the mechanistic interaction between all three SWI/SNF complexes and SAGA complexes and their epigenetic outcome.

CHAPTER FOUR: MATERIAL AND METHODS

4.1 Antibodies

REAGENT	SOURCE	IDENTIFIER
Anti-CD4-Alexa fluor 700	Thermo Fisher	Cat#56-0042-82; RRID: AB_494000
Anti-CD4-PerCP-Cy5.5	TONBO	Cat#65-0042-U100; RRID: AB_2621876
Anti-CD8-PE	Thermo Fisher	Cat#12-0081-85; RRID: AB_465532
Anti-CD8-BV510	Biolegend	Cat#100752; RRID: AB_2563057
Anti-CD45.1-BV605	Biolegend	Cat#110735; RRID:AB_11124743
Anti-CD45.2-Alexa 700	Biolegend	Cat#109822; RRID:AB_493731
Anti-Foxp3-eFluor 450	Thermo Fisher	Cat#48-5773-82; RRID:AB_1518812
Anti-NGFR-PE	Biolegend	Cat#345106; RRID:AB_2152647
Anti-NGFR-APC	Biolegend	Cat#345108; RRID:AB_10645515
Anti-Thy1.1-PE	Thermo Fisher	Cat#12-0900-83; RRID:AB_465774

Anti-CD44-BV650	Biolegend	Cat#103049; RRID:AB_2562600
Anti-CD62L-BV605	Biolegend	Cat#104438; RRID:AB_2563058
Anti-IFNg-APC	Thermo Fisher	Cat#17-7311-82; RRID:AB_469504
Ghost Viability Dye Red 780	TONBO	Cat#13-0865-T100
Anti-Foxp3	In-house	n/a
Anti-BRG1/SMARCA4	Abcam	Cat#110641; RRID:AB_10861578
Anti-BAF155/SMARCC1	Santa Cruz	Cat#sc-10756; RRID:AB_2191997
Anti-BAF47/SMARCB1	Santa Cruz	Cat#sc-166165; RRID:AB_2270651
Anti-Brd9	Active Motif	Cat#61537; RRID:AB_2614970
Anti-Pbrm1	Bethyl	Cat#A301-591A; RRID:AB_1078808
Anti-Phf10	Thermo Fisher	Cat#PA5-30678; RRID:AB_2548152
Anti-Arid1a	Santa Cruz	Cat#sc-32761; RRID:AB_673396
Anti-Histone H3K27ac	Abcam	Cat#ab4729;

		RRID:AB_2118291
Anti-IgG	Cell Signaling	Cat#2729S; RRID:AB_1031062
Anti-mouse secondary	Thermo Fisher	Cat#A21058; RRID:AB_2535724
Anti-rabbit secondary	Thermo Fisher	Cat#SA535571; RRID:AB_2556775
Anti-mouse IL2	BIO-X-CELL	Cat#BE0043 RRID:AB_1107702

4.2 Recombinant DNA

REAGENT	**SOURCE**	**IDENTIFIER**
pSIR-dsRed-Express2	Addgene	Cat#51135
pSIRG-NGFR	This paper	n/a
pSIRG-GFP	This paper	n/a
pCL-Eco	Addgene	Cat#12371
lentiCRISPRv2-Brie library	Addgene	Cat#73632
pSIRG-NGFR-Brie library	This paper	n/a
pSIRG-NGFR-sgFoxp3 Target: TCTACCCACAGGGATCAATG	This paper	n/a
pSIRG-NGFR-sgCbfb Target: GCCTTGCAGATTAAGTACAC	This paper	n/a

pSIRG-NGFR-sgDnmt1 Target: TAATGTGAACCGGTTCACAG	This paper	n/a
pSIRG-NGFR-sgArid1a Target: GCAGCTGCGAAGATATCGGG	This paper	n/a
pSIRG-NGFR-sgArid1a-2 Target: TACCCAAATATGAATCAAGG	This paper	n/a
pSIRG- NGFR-sgArid1b Target: TGAGTGCAAAACTGAGCGCG	This paper	n/a
pSIRG-NGFR-sgArid1b-2 Target: CAGAACCCCAACATATAGCG	This paper	n/a
pSIRG-NGFR-sgDpf1 Target: TCTTCTACCTCGAGATCATG	This paper	n/a
pSIRG-NGFR-sgDpf2 Target: GAAGATACGCCAAAGCGTCG	This paper	n/a
pSIRG-NGFR-sgPbrm1 Target: AAAACACTTGCATAACGATG	This paper	n/a
pSIRG-NGFR-sgPbrm1-2 Target: CAATGCCAGGCACTACAATG	This paper	n/a
pSIRG-NGFR-sgArid2 Target: ACTTGCAGTAAATTAGCTCG	This paper	n/a
pSIRG-NGFR-sgBrd7 Target: CAGGAGGCAAGCTAACACGG	This paper	n/a

pSIRG-NGFR-sgPhf10 Target: GTTGCCGACAGACCGAACGA	This paper	n/a
pSIRG-NGFR-sgBrd9 Target: ATTAACCGGTTTCTCCCGGG	This paper	n/a
pSIRG-NGFR-sgBrd9-2 Target: GGAACACTGCGACTCAGAGG	This paper	n/a
pSIRG-NGFR-sgGltscr1 Target: GTTCTGTGTAAAATCACACT	This paper	n/a
pSIRG-NGFR-sgGltscr1l Target: ATGGCTTTATGCAACACGTG	This paper	n/a
pSIRG-NGFR-sgSmarcd1 Target: CAATCCGGCTAAGTCGGACG	This paper	n/a
pSIRG-NGFR-sgEny2 Target: AGAGCTAAATTAATTGAGTG	This paper	n/a
pSIRG-NGFR-sgAtxn7l3 Target: GCAGCCGAATCGCCAACCGT	This paper	n/a
pSIRG-NGFR-sgUsp22 Target: GCCATCGACCTGATGTACGG	This paper	n/a
pSIRG-NGFR-sgCcdc101 Target: CCAGGTTTCCCGATCCAGAG	This paper	n/a
pSIRG-NGFR-sgTada3 Target: GAAGGTCTGTCCCCGCTACA	This paper	n/a

pSIRG-NGFR-sgTada1 Target: TTTCCTTCTCGACACAACTG	This paper	n/a
pSIRG-NGFR-sgTaf6l Target: TCATGAAACACACCAAACGA	This paper	n/a
pSIRG-NGFR-sgSupt20 Target: TTAGTAGTCAATCTGTACCC	This paper	n/a
pSIRG-NGFR-sgSupt5 Target: GATGACCGATGTACTCAAGG	This paper	n/a
pSIRG-NGFR-sgNT Target: AAAAAGTCCGCGATTACGTC	This paper	n/a
pSIRG-GFP-sgBrd9 Target: ATTAACCGGTTTCTCCCGGG	This paper	n/a
pSIRG-GFP-sgNT Target: AAAAAGTCCGCGATTACGTC	This paper	n/a
MSCV-IRES-GFP (MIGR)	Addgene	Cat#27490
MIGR-Foxp3	The laboratory of Alexander Rudensky	n/a

4.3 Chemicals, Peptides, and Recombinant Proteins

REAGENTS	**SOURCE**	**IDENTIFIER**
Human IL-2	Peprotech	Cat#200-02
Mouse IL-2	Biolegend	Cat#575408
dBRD9	Tocris	Cat#6606

NEBuilder HIFI assembly	NEB	Cat#E2621S
BbsI-HF	NEB	Cat#R3539S
Q5 High-Fidelity DNA polymerase	NEB	Cat#M0491
Ficoll-Paque 1.084	GE Health	Cat#17-5446-02
FuGENE 6 HD transfection reagent	Promega	Cat#E2311
Foxp3 Fix/Perm buffer	Thermo Fisher	Cat#00-5523-00
CellTrace Violet	Thermo Fisher	Cat#C34571

4.4 Cell lines

RESOURCE	**SOURCE**	**IDENTIFIER**
HEK293T	ATCC	Cat#CRL-11268
MC38	The laboratory of Susan Keach	n/a

4.5 Software and Algorithms

RESOURCE	**SOURCE**
MAGeCK	https://sourceforge.net/p/mageck/wiki/Home/ (Li et al., 2014a)
MAGeCK-VISPR	https://bitbucket.org/liulab/mageck-vispr (Li et al., 2015)
EnhancedVolcano R script	https://github.com/kevinblighe/EnhancedVolcano)
sgRNA distribution histogram R script	(Shifrut et al., 2018)

Metascape	(Zhou et al., 2019)
Cluster 3.0	http://bonsai.hgc.jp/~mdehoon/software/cluster/software.htm
HOMER	http://homer.ucsd.edu/homer/
Gene Set Enrichment Analysis (GSEA)	https://www.gsea-msigdb.org/gsea/index.jsp (Mootha et al., 2003; Subramanian et al., 2005)
Cutadapt	http://cutadapt.readthedocs.io/en/stable/
Samtools	http://htslib.org (Li et al., 2009)
Picard	http://broadinstitute.github.io/picard
BWA Aligner	http://bio-bwa.sourceforge.net (Li and Durbin, 2009)
Macs2	http://pypi.org/project/MACS2

4.6 Mice

C57BL/6 Rosa-Cas9/Foxp3$^{Thy1.1}$ mice were generated by crossing Rosa26-LSL-Cas9 mice(Platt et al., 2014) (The Jackson Laboratory #024857) with Foxp3$^{Thy1.1}$ reporter mice(Liston et al., 2008). Male Cas9/Foxp3$^{Thy1.1}$ mice at 8-12 weeks age were used to isolate Treg cells for the CRISPR screen, and no gender preference was given for other experiments. C57BL.6 Ly5.1^{+} congenic mice and Rag1$^{-/-}$ mice purchased from the Jackson Laboratory were used for Treg suppression assay and adoptive T cell transfer in colitis and tumor models. All mice were bred and housed in the specific pathogen-free facilities at the Salk Institute for Biological Studies and were conducted

under the regulation of the Institutional Animal Care and Use Committee (IACUC) and institutional guidelines.

4.7 Retroviral vectors and sgRNA library construction

Self-inactivating retroviral vector pSIRG-NGFR was generated by modifying pSIR-dsRed-Express2(Fujita and Fujii, 2014) (Addgene #51135), which enables us to clone sgRNA as efficient as lentiCRISPRv2, to enrich transduced cells via magnetic beads isolation, and to perform intracellular staining without losing transduced reporter marker. We first mutated all BbsI sites in pSIR-dsRed-Express2, then inserted a sgRNA expressing cassette containing the U6 promoter, guide RNA scaffold and a 500bp filler embedded with BbsI cloning site. The dsRed cassette was replaced by cDNA sequence of human NGFR with truncated intracellular domain. We also generated pSIRG vector with GFP (pSIRG-GFP) for the purpose of T cells transfer in tumor study, minimizing potential immune rejection. The pSIRG-GFP was generated by cutting pSIRG-NGFR with XcmI to remove NGFR cassette and replaced by GFP cDNA by Gibson cloning. For cloning single guide RNA into the pSIRG vector, an annealed sgRNA oligos can be directly inserted into BbsI-digested pSIRG-NGFR by T4 ligation similar to the cloning method utilized by lentiCRISPRv2(Sanjana et al., 2014). To create a pooled sgRNA library in pSIRG-NGFR, we first amplified sgRNA sequences from an optimized mouse CRISPR sgRNA library lentiCRISPRv2-Brie (Addgene #73632). A total of eight 50 µL PCR reactions were performed to maximize coverage of sgRNA complexity. Each 50 µL PCR reaction contained Q5 High-Fidelity DNA polymerase and buffer (NEB #M0491), 15ng of lentiCRISPRv2-Brie, and targeted primers (Forward:

GGCTTTATATATCTTGTGGAAAGGACGAAACACCG, Reverse: CTAGCCTTATTTTAACTTGCTATTTCTAGCTCTAAAAC). PCR was performed at 98°C denature, 67°C annealing, 72°C extension for 12 cycles. The sgRNA library amplicons were then combined and separated in 2 % agarose gel, and purified by the QIAquick Gel Extraction Kit (Qiagen #28704). The purified sgRNA amplicons was inserted into the BbsI-digested pSIRG-NGFR by NEBuilder HIFI assembly (NEB #E2621S). The sgRNA representative of the retroviral CRISPR library (pSIRG-NGFR-Brie) was validated by deep sequencing and comparing to the original lentiCRISPRvs-Brie. The coverage of the new pSIRG-NGFR sgRNA library was evaluated by the PinAPL-Py program (Spahn et al., 2017) .

4.8 T cell isolation and culture

For large scale Treg culture, we first expanded Treg in Rosa-Cas9/Foxp3$^{Thy1.1}$ mice by injecting IL-2:IL-2 antibody immune complex according protocol described in Webster KE et. al(Webster et al., 2009). Spleen and lymph node Treg cells were labeled with PE-conjugated Thy1.1 antibody and isolated by magnetic selection using anti-PE microbeads (Mitenyl #130-048-801). All isolated Treg cells were activated by plate bound anti-CD3 and anti-CD28 antibodies and cultured with X-VIVO 20 media (LONZA #04-448Q) supplemented by 1X Pen/Strep, 1X Sodium pyruvate, 1X HEPES, 1X GlutaMax, 55 µM beta-mercaptoethanol in the presence of IL-2 at 500 U/mL. For experiments with Brd9 degradation, Treg cells were treated at day 0 with 2.5 µM dBRD9 (Tocris #6606) and cultured for four days for RNA- and ChIP-seq and 0.16-10 µM treated at day 0 and cultured dBRD9 for four days for Foxp3 MFI, cell viability and cell

proliferation assays. Live cells were enriched by Ficoll-Paque 1.084 (GE Health 17-5446-02) for RNA-seq and ChIP-seq.

4.9 Retroviral production and T cell transduction

HEK293T cells were seeded in 6-wells plate at 0.5 million cells per 2mL DMEM media supplemented by 10% FBS, 1% Pen/Strep, 1X GlutaMax, 1X Sodium Pyruvate, 1X HEPES, and 55 μM beta-mercaptoethanol. One day later, cells from each well was transfected with 1.2 μg of targeting vector pSIRG-NGFR and 0.8 μg of packaging vector pCL-Eco (Addgene, #12371) by using 4 μL of FuGENE HD transfection reagent (Promega #E2311) according manufactured protocol. Cell culture media was replaced by 3 mL fresh DMEM complete media at 24 hours and 48 hours after transfection. The retroviral supernatant was collected at 48 and 72 hours post transfection for T cell infection. For experiments with CRISPR sgRNA targeting, Cas9+ Treg cells were first seeded in 24-wells plate coated with CD3 and CD28 antibodies. At 24 hour post-activation, 70% of Treg media from each well was replaced by retroviral supernatant, supplemented with 4 μg/mL Polybrene (Milipore # TR-1003-G), and spun in a benchtop centrifuge at 1,258 x g for 90 minutes at 32°C. After centrifugation, Treg media was replaced with fresh media supplemented with IL-2 and cultured for another three days. Transduced cells were analyzed for Foxp3 and cytokine expression in eBioscience Fix/Perm buffer (eBioscience #00-5523-00) using flow cytometry. Transduced NGFR+ cells were FACS-sorted for subsequent RNA- and ChIP-seq experiments.

4.10 Genome-wide CRISPR screen in Treg

Approximately 360 million Treg cells isolated from Rosa-Cas9/Foxp3$^{Thy1.1}$ mice were used for the Treg screen. On day 0, Treg cells were seeded at 1x10^6 cells/mL into 24-wells plate coated with anti-CD3/28 and cultured with X-VIVO complete media with IL-2 (500 U/ml). On day 1, sgRNA retroviral library transduction was performed with a MOI<0.2. On day 3, approximately 4 million (~50X coverage) NGFR$^+$ transduced cells were collected in three replicates as the starting state sgRNA input. Treg cells reached confluence on day 4. NGFR+ transduced cells were isolated via magnetic selection by anti-PE beads (Mitenyl #130-048-801), and then plated onto new 24-wells plates coated with anti-CD3/CD28, and cultured in X-VIVO complete media with IL-2 (500 U/ml). On day 6, approximately 4 million NGFR+ transduced cells were collected in three replicates as the ending state sgRNA output. The remaining cells were fixed, permeabilized, and stained for intracellular Foxp3. Approximately 2 million Foxp3^{hi} (top 20%) and 2 million Foxp3^{lo} (bottom 20%) cell populations were sorted in three replicates by a FACS Aria cell sorter for genomic DNA extraction and library construction.

4.11 Preparation of sgRNA amplicons for Next-Generation Sequencing

To extract genomic DNA, we first lysed cells with homemade digestion buffer (100mM NaCl, 10mM Tris, 25mM EDTA, 0.5% SDS, 0.1mg/mL Proteinase K) overnight in 50 °C. On the following day, the lysed sample was mixed with phenol: chloroform: isoamyl alcohol (25:24:1, v/v) in 1:1 ratio, and spun at 6000rpm for 15 min at room temperature. The supernatant containing genomic DNA was transferred into a new tube and mixed with twice volume of 100% ethanol, then spun at 12,500 rpm for 5 min in

room temperature to precipitate DNA. Supernatant was removed, and the precipitated DNA was dissolved in ddH_2O. DNA concentration was measured by Nanodrop. To generate sgRNA amplicons from extracted genomic DNA, we used a two-step PCR protocol which was adopted from the protocol published by *Shalem et. al. (Shalem et al., 2014)*. We performed eight 50 µL PCR reactions containing 2 µg genomic DNA, NEB Q5 polymerase, and buffer, and targeted primers (Forward: AATGGACTATCATATGCTTACCGTAACTTGAAAGTATTTCG, Reverse: ATCACACAAAGAGCTCTACTGCTAGCTAATAAGATAATTTG). PCR was performed at 98°C denature, 70°C annealing, 15s extension for 20 cycles. The products from the first PCR were pooled together, and purified by AMPure XP SPRI beads according to manufacturer's protocol, and quantified by Qubit dsDNA HS assay. For the second round PCR, we performed eight 50 µL PCR reactions containing 2 ng purified 1st round PCR product, barcoded primer (see primer set from *(Shalem et al., 2014)*, Priming site of reverse primer was changed to CTTCCCTCGACGAATTCCCAAC), NEB Q5 polymerase, and buffer. PCR was performed at 98°C denature, 70°C annealing, 15 s extension for 12 cycles. The 2nd round PCR products were pooled, purified by AMPure XP SPRI beads, quantified by Qubit dsDNA HS assay, and sequenced by NEXTSeq sequencer at single end 75 bp (SE75).

4.12 In vitro Treg suppression assay

Treg cells were transduced by retrovirus expressing sgRNA targeting gene of interest and cultured in X-VIVO complete media supplemented with IL-2 (500 U/ml). Four days after transduction, transduced cells were sorted and mixed with FACS sorted

CD45.1+ naive CD4 T cells ($CD4^+$ $CD25^-$ $CD44^{lo}$ $CD62L^{hi}$) labeled with CellTrace Violet (Thermo Fisher Scientific #C34571) in different ratio in the presence of irradiated T cell depleted spleen cells as antigen-presenting cells (APC). Three days later, Treg suppression function was measured by the percentage of non-dividing cells within the $CD45.1^+$ effector T cell population. For dBRD9 treatment experiment, dBRD9 was first dissolved in DMSO (10 mM stock) and added into Treg:Teff:APC mixture at 2.5 μM. For Foxp3 overexpression rescue experiment, Treg cells were first transduced with sgNT or sgBrd9 at 24 hour post-activation, and then transduced with MIGR empty vector or MIGR-Foxp3 at 48 hour post-activation. Double transduced Treg cells were FACS sorted on day 4 based on NGFR+ and GFP+ markers and then mixed with CellTrace labeled effector T cells in the presence of APC. Treg suppression readout was measured after three days of co-culture.

4.13 Adoptive T cells transfer-induced colitis model

Treg cells were transduced by retrovirus expressing sgRNA targeting gene of interest, and cultured in X-VIVO complete media and IL-2 (500 U/ml). Four days after transduction, the $NGFR^+$ transduced Treg cells were FACS sorted before transferred into recipient mice. To induce colitis, 2 million effector T cells ($CD45.1^+$ $CD4^+$ $CD25^-$ $CD45RB^{hi}$) and 1 million sgRNA transduced Treg cells ($CD45.2^+$ $CD4^+$ $Thy1.1^+$ $NGFR^+$) were mixed together and transferred into *Rag1*$^{-/-}$ recipient mice. The body weight of recipient mice was monitored weekly for signs of wasting symptoms. Mice were harvested 7 weeks after T cell transfer. Spleens were used for profiling immune cell populations by FACS. Colons were collected for histopathological analysis.

4.14 Adoptive T cells transfer and MC38 tumor model

Similar to the “Adoptive T cells transfer-induced colitis model”, Treg cells were activated *in vitro* and transduced with pSIRG-GFP expressing sgNT or sgBrd9. Four days after transduction, the GFP^+ transduced Treg were FACS sorted. Concurrently, Treg depleted CD4 and CD8 T cells isolated from Rosa-Cas9/$Foxp3^{Thy1.1}$ mice were used as effector T cells. A total of 1 million pSIRG-sgRNA transduced GFP+ Treg cells, 1 million effector CD8 T cells, and 2 million Treg-depleted CD4 T cells were mixed and transferred into *Rag1*$^{-/-}$ recipient mice. on the following day, mice were implanted with 0.5 million MC38 cells (a kind gift from the laboratory of Susan Kaech) by subcutaneous injection on the flank of mouse. When palpable tumor appeared, tumor size was measured every two day by electronic calipers. At the end point, spleen and tumor were collected for immune profiling. For tumor processing, tumor tissues were minced into small pieces and digested with 0.5 mg/mL Collagenase IV (Sigma #C5138) and DNAase I (Roche #4716728001) for 20 minutes and passed through 0.75 μm cell strainer to collect single cell suspension. Isolated cells were stimulated with PMA/Ionomycin and Golgi plug for 5 hours, and then were subjected to Foxp3 and cytokines staining with eBioscience Fix/Perm buffer (eBioscience #00-5523-00).

4.15 Nuclear protein extraction

Nuclear lysates were collected from Treg cells following a revised Dignam protocol(Andrews and Faller, 1991). After cellular swelling in Buffer A (10 mM Hepes pH 7.9, 1.5 mM $MgCl_2$, 10 mM KCl) supplemented with 1 mM DTT, 1 mM PMSF, 1 μM

pepstatin, 10 μM leupeptin and 10 μM chymostatin, cells were lysed by homogenization using a 21-gauge needle with six to eight strokes. If lysis remained incomplete, cells were treated with 0.025 - 0.05% Igepal-630 for ten minutes on ice prior to nuclei collection. Nuclei were spun down at 700 x g for five minutes then resuspended in Buffer C (20 mM Hepes pH 7.9, 20% glycerol, 420 mM NaCl, 1.5 mM $MgCl_2$, 0.2 mM EDTA) supplemented with 1 mM DTT, 1 mM PMSF, 1 μM pepstatin, 10 μM leupeptin and 10 μM chymostatin. After thirty minutes of end-to-end rotation at 4°C, the sample was clarified at 21,100 x g for ten minutes. Supernatant was collected, flash frozen in liquid nitrogen and stored in the -80°C freezer.

4.16 Co-Immunoprecipitation

Nuclear lysates were thawed on ice then diluted with two-thirds of original volume of 50 mM Tris-HCl pH 8, 0.3% NP-40, EDTA, $MgCl_2$ to bring down the NaCl concentration. Proteins were quantified using Biorad DC Protein Assay (Cat #5000112) according to manufacturer's instructions. For the co-IP reaction, 200-300 μg of proteins were incubated with antibody against normal IgG, Smarca4, Brd9, Arid1a or Phf10 overnight at 4°C, with end-to-end rotation. Precipitated proteins were bound to 50:50 Protein A: Protein G Dynabeads (Invitrogen) for one to two hours and washed extensively with IP wash buffer (50 mM Tris pH 8, 150 mM NaCl, 1 mM EDTA, 10% glycerol, 0.5% Triton X100). Proteins were eluted in SDS-PAGE loading solution with boiling for five minutes and analyzed by western blotting.

4.17 Western blot

Protein samples were run on 4-12% Bis-Tris gels (Life Technologies). After primary antibody incubation which is typically done overnight at 4°C, blots were probed with 1:20,000 dilution of fluorescently-labeled secondary antibodies in 2% BSA in PBST (1X Phospho-buffered saline with 0.1% Tween-20) for an hour at room temperature (RT). Fluorescent images were developed using Odyssey and analyzed using Image Studio 2. Protein quantitation was performed by first normalizing the measured fluorescence values of the proteins of interest against the loading control (TBP) then normalizing against the control sample (vehicle treated).

4.18 RNA-seq sample preparation

RNA from 1-3 x 10^6 cells was extracted and purified with TRIzol reagent (Thermo Fisher) according to manufacturer's instructions. RNA-seq libraries were prepared using Illumina TruSeq Stranded mRNA kit following manufacturer's instructions with 5 µg of input RNA.

4.19 ChIP-seq sample preparation

Treg cells were collected and cross-linked first in 3 mM disuccinimidyl glutarate (DSG) in 1X PBS for thirty minutes then in 1% formaldehyde for another ten minutes, both at RT, for chromatin binding protein ChIP or in 1% formaldehyde only for histone modification ChIP. After quenching the excess cross-linker with a final concentration of 125 mM glycine, the cells were washed in 1X PBS, pelleted, flash-frozen in liquid nitrogen, and stored at -80°C. Cell pellets were thawed on ice and incubated in lysis

solution (50 mM HEPES-KOH pH 8, 140 mM NaCl, 1 mM EDTA, 10% glycerol, 0.5% NP40, 0.25% Triton X-100) for ten minutes. The isolated nuclei were washed with wash solution (10 mM Tris-HCl pH 8, 1 mM EDTA, 0.5 mM EGTA, 200 mM NaCl) and shearing buffer (0.1% SDS, 1 mM EDTA, 10 mM Tris-HCl pH 8) then sheared in a Covaris E229 sonicator for ten minutes to generate DNA fragments between ~ 200-1000 base pairs (bp). After clarification of insoluble material by centrifugation, the chromatin was immunoprecipitated overnight at 4°C with antibodies against Foxp3, Smarca4, Brd9, Phf10 or H3K27ac. The next day, the antibody bound DNA was incubated with Protein A+G Dynabeads (Invitrogen) in ChIP buffer (50 mM HEPES-KOH pH 7.5, 300 mM NaCl, 1 mM EDTA, 1% Triton X-100, 0.1% DOC, 0.1% SDS), washed and treated with Proteinase K and RNase A. Cross-linking was reversed by incubation at 55°C for two and a half hours. Purified ChIP DNA was used for library generation (NuGen Ovation Ultralow Library System V2) according to manufacturer's instructions for subsequent sequencing.

4.20 ATAC-seq sample preparation

ATAC-seq was performed according to previously published protocol (Corces et al., 2017). Briefly, Tregs transduced with either sgNT or sgBrd9 were subjected to Ficoll gradient purification to remove dead cells and ensure capture of cells that were 99% viable. 50,000 Treg cells were collected in duplicates per genotype and washed first with cold 1X PBS then with Resuspension buffer (RSB; 10 mM Tris-HCl pH 7.4, 10 mM NaCl, 3 mM $MgCl_2$). Cells were lysed in 50 µL of RSB supplemented with 0.1% NP40, 0.01% Digitonin and 0.1% Tween 20 for 3 minutes on ice then diluted with 1 mL of RSB

with 0.1% Tween 20. Nuclei were isolated by centrifugation at 500 x g for ten minutes then resuspended in 50 µL of transposition mix (25 µL 2x Illumina Transposase buffer, 2.5 µL Illumina Tn5 Transposase, 16.5 µL PBS, 0.5 µL 1% Digitonin, 0.5 µL 10% Tween 20, 5 µL water) for 30 minutes at 37C in a thermomixer with shaking at 1,000 rpm. Reactions were cleaned up with Qiagen Min-Elute columns. ATAC-seq libraries were prepared as described previously (Buenrostro et al., 2013). Briefly, purified DNA was ligated with adapters and amplified to a target concentration of 20 µL at 4 nM. Libraries were size selected using AMPure XP beads (Beckman) and sequenced using NextSeq for paired end 42 bp (PE42) sequencing.

4.21 Data analysis of pooled CRISPR screen

The screening hit identification and quality control was performed by MAGeCK-VISPR program(Li et al., 2015; Li et al., 2014a). The abundance of sgRNA from a sample fastq file was first quantified by MAGeCK “Count” module to generate a read count table. For hit calling, we used MAGeCK “test” module to generate a gene-ranking table that reporting RRA gene ranking score, p-value, and log2 fold change. The size factor for normalization was adjusted according to1000 non-targeting control assigned in the screen library. All sgRNAs that are zero read were removed from RRA analysis. The log2 fold change of a gene was calculated from a mean of 4 sgRNA targeting per gene. The scatter plots showing the screen results were generated by using the R script EnhancedVolcano (https://github.com/kevinblighe/EnhancedVolcano). The R script that generated the sgRNA distribution histogram was provided by E. Shifrut and A. Marson (UCSF)(Shifrut et al., 2018). A gene list from Foxp3 regulators (either positive or

negative) without affecting cell proliferation was subjected to Gene Ontology analysis using Metascape(Zhou et al., 2019). Genes were analyzed for enrichment for Functional Set, Pathway, and Structural Complex.

4.22 Colon histopathological analysis

Histopathological analysis was performed in a blinded manner and scored using the following criteria. Eight parameters were used that include (i) the degree of inflammatory infiltrate in the LP (0-3); (ii) Goblet cell loss (0–2); (iii) reactive epithelial hyperplasia/atypia with nuclear changes (0–3); (iv) the number of IELs in the epithelial crypts (0–3); (v) abnormal crypt architecture (distortion, branching, atrophy, crypt loss) (0–3); (vi) number of crypt abscesses (0–2); (vii) mucosal erosion to frank ulcerations (0–2) and (viii) submucosal spread to transmural involvement (0-2). The severity of lesion was scored independently in 3 regions (proximal, middle and distal colon) over a maximal score of 20. The overall colitis score was based as the average of each regional score (maximal score of 20).

4.23 RNA-seq analysis

Single-end 50 bp reads were aligned to the mouse genome mm10 using STAR alignment tool (V2.5)(Dobin et al., 2013). RNA expression was quantified as raw integer counts using analyzeRepeats.pl in HOMER(Heinz et al., 2010) using the following parameters: -strand both -count exons -condenseGenes -noadj. To identify differentially expressed genes, we performed getDiffExpression.pl in HOMER, which uses the DESeq2 R package to calculate the biological variation within replicates. Cut-offs were

set at log2 FC = 0.585 and FDR at 0.05 (Benjamin-Hochberg). Principal Component Analysis (PCA) was performed with the mean of transcript per million (TPM) values using Cluster 3.0 with the following filter parameters: at least one observation with absolute value equal or greater than two and gene vector of four. TPM values were log transformed then centered on the mean.

4.24 Gene Set Enrichment Analysis

GSEA software(Mootha et al., 2003; Subramanian et al., 2005) was used to perform the analyses with the following parameters: number of permutations = 1000; enrichment statistic = weighted; and metric for ranking of genes = difference of classes (Input RNA-seq data was log-transformed). For Figure 14G, input RNA-seq data contained the normalized log-transformed reads of the 1,325 differentially expressed genes (DEGs) in sgFoxp3/sgNT Treg cells. The compiled gene list included GSEA Gene Ontology, Immunological Signature, Curated Gene, and the up and down DEGs in sgBrd9/sgNT Treg cells. The resulting normalized enrichment scores and FWER p values were combined to generate the graph.

4.25 ChIP-seq analysis

Single-end 50 bp or paired-end 42 bp reads were aligned to mouse genome mm10 using STAR alignment tool (V2.5)(Dobin et al., 2013). ChIP-Seq peaks were called using findPeaks within HOMER using parameters for histone (-style histone) or transcription factor (-style factor) (Christopher Benner, HOMER, http://homer.ucsd.edu/homer/index.html, 2018). Peaks were called when enriched >

two-fold over input and > four-fold over local tag counts, with FDR 0.001 (Benjamin-Hochberg). For histone ChIP, peaks within a 1000 bp range were stitched together to form regions. Differential ChIP peaks were found by merging peaks from control and experiment groups and called using getDiffExpression.pl with fold change ≥ 1.5 or ≤ -1.5, Poisson p value < 0.0001.

For k-means clustering analysis in Figure S6D, Foxp3 ChIP-seq tags were quantified at the sites that significantly lose Foxp3 binding in sgBrd9, MIGR compared to sgNT, MIGR using the annotatePeaks.pl command in HOMER with -size given. Log2FC values were calculated for sgBrd9, MIGR/sgNT, MIGR and sgBrd9, Foxp3/sgNT, MIGR. k-means clustering was performed using Gene Cluster 3.0 and visualized using Java TreeView.

For gene expression analysis in Figure S6F, Foxp3 ChIP-seq tags were quantified at the union of sites bound by Foxp3 in sgNT and sgBrd9 using the annotatePeaks.pl command in HOMER with size -given and each site was annotated to a gene by mapping to the nearest TSS. Sites were ranked from least to largest Foxp3 ChIP-seq Log2FC in sgBrd9 vs sgNT and divided into quartiles. Gene expression for the genes in the top and bottom quartiles (Brd9-dependent and -independent, respectively) was then plotted using RNA-seq data from Treg cells transduced with sgBrd9, sgSmarcd1, or sgPbrm1 compared to sgNT. Statistical analyses were performed using unpaired two-tailed Student's t test (ns: $p \geq 0.05$, *$p < 0.05$, **$p < 0.01$) in Graphpad Prism.

4.26 Motif analysis

Sequences within 200 bp of peak centers were compared to motifs in the HOMER database using the findMotifsGenome.pl command using default fragment size and motif length parameters. Random GC content-matched genomic regions were used as background. Enriched motifs are statistically significant motifs in input over background by a p-value of less than 0.05. P-values were calculated using cumulative binomial distribution.

4.27 ATAC-seq analysis

ATAC-seq data analysis used the following tools and versions: cutadapt (v2.4), samtools (v1.9), Picard (v1.7.1), BWA (v0.7.12), macs2 (v2.1.2), and HOMER (v4.11). Paired end 42 bp reads were trimmed using cutadapt to remove Nextera adapter sequences then aligned to the reference mouse genome mm10 using BWA. The following were filtered out using Picard and samtools: duplicate reads, mitochondrial reads, low quality reads (Q < 20), and improperly paired or unpaired reads. Quality was assessed by calculating Fraction of Reads In Peaks (FRIP Score) which were > 40% for all samples. TSS enrichment was determined using mm10 Refseq TSSs. Broad and narrow peaks were called using macs2 using the following parameters: --slocal 1000 –qvalue 0.05 -f BAMPE. Differentially accessible sites were determined using getDifferentialPeaksReplicates.pl command in HOMER using the union of peaks in sgNT and sgBrd9 with the following parameters: edgeR, fold change cutoff 1.5, adjusted p value < 0.05.

4.28 Data availability

RNA-seq, ChIP-seq, and ATAC-seq data that support the findings of this study have been deposited in the Gene Expression Omnibus under the accession code GSE129846 [https://www.ncbi.nlm.nih.gov/geo/query/acc.cgi?acc=GSE129846].

The contents and data presented in this chapter is adapted from an article published in 2020 in the journal Immunity titled “A Genome-wide CRISPR Screen Reveals a Role for the Non-canonical Nucleosome-Remodeling BAF Complex in Foxp3 Expression and Regulatory T Cell Function” The authorship of this paper is: Chin-San Loo, Jovylyn Gatchalian, Yuqiong Liang, Mathias Leblanc, Mingjun Xie, Josephine Ho, Bhargav Venkatraghavan, Diana C Hargreaves, and Ye Zheng

REFERENCES

Alpsoy, A., and Dykhuizen, E.C. (2018). Glioma tumor suppressor candidate region gene 1 (GLTSCR1) and its paralog GLTSCR1-like form SWI/SNF chromatin remodeling subcomplexes. The Journal of biological chemistry *293*, 3892-3903.

Andrews, N.C., and Faller, D.V. (1991). A rapid micropreparation technique for extraction of DNA-binding proteins from limiting numbers of mammalian cells. Nucleic Acids Res *19*, 2499.

Asano, M., Toda, M., Sakaguchi, N., and Sakaguchi, S. (1996). Autoimmune disease as a consequence of developmental abnormality of a T cell subpopulation. J Exp Med *184*, 387-396.

Bennett, C.L., Christie, J., Ramsdell, F., Brunkow, M.E., Ferguson, P.J., Whitesell, L., Kelly, T.E., Saulsbury, F.T., Chance, P.F., and Ochs, H.D. (2001). The immune dysregulation, polyendocrinopathy, enteropathy, X-linked syndrome (IPEX) is caused by mutations of FOXP3. Nat Genet *27*, 20-21.

Brunkow, M.E., Jeffery, E.W., Hjerrild, K.A., Paeper, B., Clark, L.B., Yasayko, S.A., Wilkinson, J.E., Galas, D., Ziegler, S.F., and Ramsdell, F. (2001). Disruption of a new forkhead/winged-helix protein, scurfin, results in the fatal lymphoproliferative disorder of the scurfy mouse. Nat Genet *27*, 68-73.

Buenrostro, J.D., Giresi, P.G., Zaba, L.C., Chang, H.Y., and Greenleaf, W.J. (2013). Transposition of native chromatin for fast and sensitive epigenomic profiling of open chromatin, DNA-binding proteins and nucleosome position. Nat Methods *10*, 1213-1218.

Burchill, M.A., Yang, J., Vogtenhuber, C., Blazar, B.R., and Farrar, M.A. (2007). IL-2 receptor beta-dependent STAT5 activation is required for the development of Foxp3+ regulatory T cells. Journal of immunology *178*, 280-290.

Chaiyachati, B.H., Jani, A., Wan, Y., Huang, H., Flavell, R., and Chi, T. (2013). BRG1-mediated immune tolerance: facilitation of Treg activation and partial independence of chromatin remodelling. EMBO J *32*, 395-408.

Chapman, N.M., Zeng, H., Nguyen, T.M., Wang, Y., Vogel, P., Dhungana, Y., Liu, X., Neale, G., Locasale, J.W., and Chi, H. (2018). mTOR coordinates transcriptional programs and mitochondrial metabolism of activated Treg subsets to protect tissue homeostasis. Nature communications *9*, 2095.

Chatila, T.A., Blaeser, F., Ho, N., Lederman, H.M., Voulgaropoulos, C., Helms, C., and Bowcock, A.M. (2000). JM2, encoding a fork head-related protein, is mutated in X-linked autoimmunity-allergic disregulation syndrome. J Clin Invest *106*, R75-81.

Chen, W., Jin, W., Hardegen, N., Lei, K.J., Li, L., Marinos, N., McGrady, G., and Wahl, S.M. (2003). Conversion of peripheral CD4+CD25- naive T cells to CD4+CD25+

regulatory T cells by TGF-beta induction of transcription factor Foxp3. J Exp Med *198*, 1875-1886.

Chen, Z., Barbi, J., Bu, S., Yang, H.Y., Li, Z., Gao, Y., Jinasena, D., Fu, J., Lin, F., Chen, C., Zhang, J., Yu, N., Li, X., Shan, Z., Nie, J., Gao, Z., Tian, H., Li, Y., Yao, Z., Zheng, Y., Park, B.V., Pan, Z., Zhang, J., Dang, E., Li, Z., Wang, H., Luo, W., Li, L., Semenza, G.L., Zheng, S.G., Loser, K., Tsun, A., Greene, M.I., Pardoll, D.M., Pan, F., and Li, B. (2013). The ubiquitin ligase Stub1 negatively modulates regulatory T cell suppressive activity by promoting degradation of the transcription factor Foxp3. Immunity *39*, 272-285.

Chinen, T., Kannan, A.K., Levine, A.G., Fan, X., Klein, U., Zheng, Y., Gasteiger, G., Feng, Y., Fontenot, J.D., and Rudensky, A.Y. (2016). An essential role for the IL-2 receptor in Treg cell function. Nat Immunol *17*, 1322-1333.

Corces, M.R., Trevino, A.E., Hamilton, E.G., Greenside, P.G., Sinnott-Armstrong, N.A., Vesuna, S., Satpathy, A.T., Rubin, A.J., Montine, K.S., Wu, B., Kathiria, A., Cho, S.W., Mumbach, M.R., Carter, A.C., Kasowski, M., Orloff, L.A., Risca, V.I., Kundaje, A., Khavari, P.A., Montine, T.J., Greenleaf, W.J., and Chang, H.Y. (2017). An improved ATAC-seq protocol reduces background and enables interrogation of frozen tissues. Nat Methods *14*, 959-962.

Cortez, J.T., Montauti, E., Shifrut, E., Gatchalian, J., Zhang, Y., Shaked, O., Xu, Y., Roth, T.L., Simeonov, D.R., Zhang, Y., Chen, S., Li, Z., Woo, J.M., Ho, J., Vogel, I.A., Prator, G.Y., Zhang, B., Lee, Y., Sun, Z., Ifergan, I., Van Gool, F., Hargreaves, D.C., Bluestone, J.A., Marson, A., and Fang, D. (2020). CRISPR screen in regulatory T cells reveals modulators of Foxp3. Nature.

Delgoffe, G.M., Kole, T.P., Zheng, Y., Zarek, P.E., Matthews, K.L., Xiao, B., Worley, P.F., Kozma, S.C., and Powell, J.D. (2009). The mTOR kinase differentially regulates effector and regulatory T cell lineage commitment. Immunity *30*, 832-844.

Delgoffe, G.M., Woo, S.R., Turnis, M.E., Gravano, D.M., Guy, C., Overacre, A.E., Bettini, M.L., Vogel, P., Finkelstein, D., Bonnevier, J., Workman, C.J., and Vignali, D.A. (2013). Stability and function of regulatory T cells is maintained by a neuropilin-1-semaphorin-4a axis. Nature *501*, 252-256.

Dobin, A., Davis, C.A., Schlesinger, F., Drenkow, J., Zaleski, C., Jha, S., Batut, P., Chaisson, M., and Gingeras, T.R. (2013). STAR: ultrafast universal RNA-seq aligner. Bioinformatics *29*, 15-21.

Doench, J.G., Fusi, N., Sullender, M., Hegde, M., Vaimberg, E.W., Donovan, K.F., Smith, I., Tothova, Z., Wilen, C., Orchard, R., Virgin, H.W., Listgarten, J., and Root, D.E. (2016). Optimized sgRNA design to maximize activity and minimize off-target effects of CRISPR-Cas9. Nat Biotechnol *34*, 184-191.

Feng, Y., Arvey, A., Chinen, T., van der Veeken, J., Gasteiger, G., and Rudensky, A.Y. (2014). Control of the inheritance of regulatory T cell identity by a cis element in the Foxp3 locus. Cell *158*, 749-763.

Feuerer, M., Hill, J.A., Kretschmer, K., von Boehmer, H., Mathis, D., and Benoist, C. (2010). Genomic definition of multiple ex vivo regulatory T cell subphenotypes. Proceedings of the National Academy of Sciences of the United States of America *107*, 5919-5924.

Fontenot, J.D., Gavin, M.A., and Rudensky, A.Y. (2003). Foxp3 programs the development and function of CD4+CD25+ regulatory T cells. Nat Immunol *4*, 330-336.

Fujita, T., and Fujii, H. (2014). Identification of proteins associated with an IFNgamma-responsive promoter by a retroviral expression system for enChIP using CRISPR. PloS one *9*, e103084.

Gaj, T., Sirk, S.J., Shui, S.L., and Liu, J. (2016). Genome-Editing Technologies: Principles and Applications. Cold Spring Harb Perspect Biol *8*.

Gatchalian, J., Malik, S., Ho, J., Lee, D.S., Kelso, T.W.R., Shokhirev, M.N., Dixon, J.R., and Hargreaves, D.C. (2018). A non-canonical BRD9-containing BAF chromatin remodeling complex regulates naive pluripotency in mouse embryonic stem cells. Nat Commun *9*, 5139.

Gebuhr, T.C., Kovalev, G.I., Bultman, S., Godfrey, V., Su, L., and Magnuson, T. (2003). The role of Brg1, a catalytic subunit of mammalian chromatin-remodeling complexes, in T cell development. The Journal of experimental medicine *198*, 1937-1949.

Germain, R.N. (2008). Special regulatory T-cell review: A rose by any other name: from suppressor T cells to Tregs, approbation to unbridled enthusiasm. Immunology *123*, 20-27.

Gershon, R.K., and Kondo, K. (1970). Cell interactions in the induction of tolerance: the role of thymic lymphocytes. Immunology *18*, 723-737.

Green, D.R., Flood, P.M., and Gershon, R.K. (1983). Immunoregulatory T-cell pathways. Annu Rev Immunol *1*, 439-463.

Heinz, S., Benner, C., Spann, N., Bertolino, E., Lin, Y.C., Laslo, P., Cheng, J.X., Murre, C., Singh, H., and Glass, C.K. (2010). Simple combinations of lineage-determining transcription factors prime cis-regulatory elements required for macrophage and B cell identities. Mol Cell *38*, 576-589.

Helmlinger, D., and Tora, L. (2017). Sharing the SAGA. Trends Biochem Sci *42*, 850-861.

Hill, J.A., Feuerer, M., Tash, K., Haxhinasto, S., Perez, J., Melamed, R., Mathis, D., and Benoist, C. (2007). Foxp3 transcription-factor-dependent and -independent regulation of the regulatory T cell transcriptional signature. Immunity *27*, 786-800.

Hori, S., Nomura, T., and Sakaguchi, S. (2003). Control of regulatory T cell development by the transcription factor Foxp3. Science *299*, 1057-1061.

Jiang, F., and Doudna, J.A. (2017). CRISPR-Cas9 Structures and Mechanisms. Annu Rev Biophys *46*, 505-529.

Josefowicz, S.Z., Lu, L.F., and Rudensky, A.Y. (2012). Regulatory T cells: mechanisms of differentiation and function. Annu Rev Immunol *30*, 531-564.

Josefowicz, S.Z., Wilson, C.B., and Rudensky, A.Y. (2009). Cutting edge: TCR stimulation is sufficient for induction of Foxp3 expression in the absence of DNA methyltransferase 1. J Immunol *182*, 6648-6652.

Khattri, R., Cox, T., Yasayko, S.A., and Ramsdell, F. (2003). An essential role for Scurfin in CD4+CD25+ T regulatory cells. Nat Immunol *4*, 337-342.

Kim, H.P., and Leonard, W.J. (2007). CREB/ATF-dependent T cell receptor-induced FoxP3 gene expression: a role for DNA methylation. The Journal of experimental medicine *204*, 1543-1551.

Kim, J.M., Rasmussen, J.P., and Rudensky, A.Y. (2007). Regulatory T cells prevent catastrophic autoimmunity throughout the lifespan of mice. Nat Immunol *8*, 191-197.

Kitagawa, Y., Ohkura, N., Kidani, Y., Vandenbon, A., Hirota, K., Kawakami, R., Yasuda, K., Motooka, D., Nakamura, S., Kondo, M., Taniuchi, I., Kohwi-Shigematsu, T., and Sakaguchi, S. (2017). Guidance of regulatory T cell development by Satb1-dependent super-enhancer establishment. Nat Immunol *18*, 173-183.

Kitoh, A., Ono, M., Naoe, Y., Ohkura, N., Yamaguchi, T., Yaguchi, H., Kitabayashi, I., Tsukada, T., Nomura, T., Miyachi, Y., Taniuchi, I., and Sakaguchi, S. (2009). Indispensable role of the Runx1-Cbfbeta transcription complex for in vivo-suppressive function of FoxP3+ regulatory T cells. Immunity *31*, 609-620.

Kojima, A., and Prehn, R.T. (1981). Genetic susceptibility to post-thymectomy autoimmune diseases in mice. Immunogenetics *14*, 15-27.

Koutelou, E., Hirsch, C.L., and Dent, S.Y. (2010). Multiple faces of the SAGA complex. Curr Opin Cell Biol *22*, 374-382.

Kronenberg, M., Steinmetz, M., Kobori, J., Kraig, E., Kapp, J.A., Pierce, C.W., Sorensen, C.M., Suzuki, G., Tada, T., and Hood, L. (1983). RNA transcripts for I-J polypeptides are apparently not encoded between the I-A and I-E subregions of the murine major histocompatibility complex. Proc Natl Acad Sci U S A *80*, 5704-5708.

Lahl, K., Loddenkemper, C., Drouin, C., Freyer, J., Arnason, J., Eberl, G., Hamann, A., Wagner, H., Huehn, J., and Sparwasser, T. (2007). Selective depletion of Foxp3+ regulatory T cells induces a scurfy-like disease. J Exp Med *204*, 57-63.

Lee, H.M., Bautista, J.L., Scott-Browne, J., Mohan, J.F., and Hsieh, C.S. (2012). A broad range of self-reactivity drives thymic regulatory T cell selection to limit responses to self. Immunity *37*, 475-486.

Lessard, J., Wu, J.I., Ranish, J.A., Wan, M., Winslow, M.M., Staahl, B.T., Wu, H., Aebersold, R., Graef, I.A., and Crabtree, G.R. (2007). An essential switch in subunit composition of a chromatin remodeling complex during neural development. Neuron *55*, 201-215.

Li, H., and Durbin, R. (2009). Fast and accurate short read alignment with Burrows-Wheeler transform. Bioinformatics *25*, 1754-1760.

Li, H., Handsaker, B., Wysoker, A., Fennell, T., Ruan, J., Homer, N., Marth, G., Abecasis, G., Durbin, R., and Genome Project Data Processing, S. (2009). The Sequence Alignment/Map format and SAMtools. Bioinformatics *25*, 2078-2079.

Li, W., Koster, J., Xu, H., Chen, C.H., Xiao, T., Liu, J.S., Brown, M., and Liu, X.S. (2015). Quality control, modeling, and visualization of CRISPR screens with MAGeCK-VISPR. Genome Biol *16*, 281.

Li, W., Xu, H., Xiao, T., Cong, L., Love, M.I., Zhang, F., Irizarry, R.A., Liu, J.S., Brown, M., and Liu, X.S. (2014a). MAGeCK enables robust identification of essential genes from genome-scale CRISPR/Cas9 knockout screens. Genome Biol *15*, 554.

Li, X., Liang, Y., LeBlanc, M., Benner, C., and Zheng, Y. (2014b). Function of a Foxp3 cis-element in protecting regulatory T cell identity. Cell *158*, 734-748.

Liston, A., Nutsch, K.M., Farr, A.G., Lund, J.M., Rasmussen, J.P., Koni, P.A., and Rudensky, A.Y. (2008). Differentiation of regulatory Foxp3+ T cells in the thymic cortex. Proceedings of the National Academy of Sciences of the United States of America *105*, 11903-11908.

Liu, Y., Zhang, P., Li, J., Kulkarni, A.B., Perruche, S., and Chen, W. (2008). A critical function for TGF-beta signaling in the development of natural CD4+CD25+Foxp3+ regulatory T cells. Nat Immunol *9*, 632-640.

Long, M., Park, S.G., Strickland, I., Hayden, M.S., and Ghosh, S. (2009). Nuclear factor-kappaB modulates regulatory T cell development by directly regulating expression of Foxp3 transcription factor. Immunity *31*, 921-931.

Michel, B.C., D'Avino, A.R., Cassel, S.H., Mashtalir, N., McKenzie, Z.M., McBride, M.J., Valencia, A.M., Zhou, Q., Bocker, M., Soares, L.M.M., Pan, J., Remillard, D.I., Lareau, C.A., Zullow, H.J., Fortoul, N., Gray, N.S., Bradner, J.E., Chan, H.M., and Kadoch, C. (2018). A non-canonical SWI/SNF complex is a synthetic lethal target in cancers driven by BAF complex perturbation. Nature cell biology *20*, 1410-1420.

Mootha, V.K., Lindgren, C.M., Eriksson, K.F., Subramanian, A., Sihag, S., Lehar, J., Puigserver, P., Carlsson, E., Ridderstrale, M., Laurila, E., Houstis, N., Daly, M.J., Patterson, N., Mesirov, J.P., Golub, T.R., Tamayo, P., Spiegelman, B., Lander, E.S., Hirschhorn, J.N., Altshuler, D., and Groop, L.C. (2003). PGC-1alpha-responsive genes involved in oxidative phosphorylation are coordinately downregulated in human diabetes. Nat Genet *34*, 267-273.

Morrissey, P.J., Charrier, K., Braddy, S., Liggitt, D., and Watson, J.D. (1993). CD4+ T cells that express high levels of CD45RB induce wasting disease when transferred into congenic severe combined immunodeficient mice. Disease development is prevented by cotransfer of purified CD4+ T cells. J Exp Med *178*, 237-244.

Nishizuka, Y., and Sakakura, T. (1969). Thymus and reproduction: sex-linked dysgenesia of the gonad after neonatal thymectomy in mice. Science *166*, 753-755.

Ortega, G., Robb, R.J., Shevach, E.M., and Malek, T.R. (1984). The murine IL 2 receptor. I. Monoclonal antibodies that define distinct functional epitopes on activated T cells and react with activated B cells. J Immunol *133*, 1970-1975.

Ouyang, W., Beckett, O., Ma, Q., and Li, M.O. (2010). Transforming growth factor-beta signaling curbs thymic negative selection promoting regulatory T cell development. Immunity *32*, 642-653.

Platt, R.J., Chen, S., Zhou, Y., Yim, M.J., Swiech, L., Kempton, H.R., Dahlman, J.E., Parnas, O., Eisenhaure, T.M., Jovanovic, M., Graham, D.B., Jhunjhunwala, S., Heidenreich, M., Xavier, R.J., Langer, R., Anderson, D.G., Hacohen, N., Regev, A., Feng, G., Sharp, P.A., and Zhang, F. (2014). CRISPR-Cas9 knockin mice for genome editing and cancer modeling. Cell *159*, 440-455.

Polansky, J.K., Kretschmer, K., Freyer, J., Floess, S., Garbe, A., Baron, U., Olek, S., Hamann, A., von Boehmer, H., and Huehn, J. (2008). DNA methylation controls Foxp3 gene expression. Eur J Immunol *38*, 1654-1663.

Powrie, F., Leach, M.W., Mauze, S., Caddle, L.B., and Coffman, R.L. (1993). Phenotypically distinct subsets of CD4+ T cells induce or protect from chronic intestinal inflammation in C. B-17 scid mice. Int Immunol *5*, 1461-1471.

Remillard, D., Buckley, D.L., Paulk, J., Brien, G.L., Sonnett, M., Seo, H.S., Dastjerdi, S., Wuhr, M., Dhe-Paganon, S., Armstrong, S.A., and Bradner, J.E. (2017). Degradation of the BAF Complex Factor BRD9 by Heterobifunctional Ligands. Angew Chem Int Ed Engl *56*, 5738-5743.

Rudra, D., Egawa, T., Chong, M.M., Treuting, P., Littman, D.R., and Rudensky, A.Y. (2009). Runx-CBFbeta complexes control expression of the transcription factor Foxp3 in regulatory T cells. Nat Immunol *10*, 1170-1177.

Sakaguchi, S. (2011). Regulatory T cells: history and perspective. Methods Mol Biol *707*, 3-17.

Sakaguchi, S., Sakaguchi, N., Asano, M., Itoh, M., and Toda, M. (1995). Immunologic self-tolerance maintained by activated T cells expressing IL-2 receptor alpha-chains (CD25). Breakdown of a single mechanism of self-tolerance causes various autoimmune diseases. J Immunol *155*, 1151-1164.

Sakaguchi, S., Takahashi, T., and Nishizuka, Y. (1982). Study on cellular events in post-thymectomy autoimmune oophoritis in mice. II. Requirement of Lyt-1 cells in normal female mice for the prevention of oophoritis. J Exp Med *156*, 1577-1586.

Sakaguchi, S., Yamaguchi, T., Nomura, T., and Ono, M. (2008). Regulatory T cells and immune tolerance. Cell *133*, 775-787.

Samstein, R.M., Arvey, A., Josefowicz, S.Z., Peng, X., Reynolds, A., Sandstrom, R., Neph, S., Sabo, P., Kim, J.M., Liao, W., Li, M.O., Leslie, C., Stamatoyannopoulos, J.A., and Rudensky, A.Y. (2012). Foxp3 exploits a pre-existent enhancer landscape for regulatory T cell lineage specification. Cell *151*, 153-166.

Sanjana, N.E., Shalem, O., and Zhang, F. (2014). Improved vectors and genome-wide libraries for CRISPR screening. Nat Methods *11*, 783-784.

Shalem, O., Sanjana, N.E., Hartenian, E., Shi, X., Scott, D.A., Mikkelson, T., Heckl, D., Ebert, B.L., Root, D.E., Doench, J.G., and Zhang, F. (2014). Genome-scale CRISPR-Cas9 knockout screening in human cells. Science *343*, 84-87.

Shifrut, E., Carnevale, J., Tobin, V., Roth, T.L., Woo, J.M., Bui, C.T., Li, P.J., Diolaiti, M.E., Ashworth, A., and Marson, A. (2018). Genome-wide CRISPR Screens in Primary Human T Cells Reveal Key Regulators of Immune Function. Cell *175*, 1958-1971 e1915.

Spahn, P.N., Bath, T., Weiss, R.J., Kim, J., Esko, J.D., Lewis, N.E., and Harismendy, O. (2017). PinAPL-Py: A comprehensive web-application for the analysis of CRISPR/Cas9 screens. Sci Rep *7*, 15854.

Subramanian, A., Tamayo, P., Mootha, V.K., Mukherjee, S., Ebert, B.L., Gillette, M.A., Paulovich, A., Pomeroy, S.L., Golub, T.R., Lander, E.S., and Mesirov, J.P. (2005). Gene set enrichment analysis: a knowledge-based approach for interpreting genome-wide expression profiles. Proceedings of the National Academy of Sciences of the United States of America *102*, 15545-15550.

Sun, I.H., Oh, M.H., Zhao, L., Patel, C.H., Arwood, M.L., Xu, W., Tam, A.J., Blosser, R.L., Wen, J., and Powell, J.D. (2018). mTOR Complex 1 Signaling Regulates the Generation and Function of Central and Effector Foxp3(+) Regulatory T Cells. Journal of immunology *201*, 481-492.

Suri-Payer, E., Amar, A.Z., Thornton, A.M., and Shevach, E.M. (1998). CD4+CD25+ T cells inhibit both the induction and effector function of autoreactive T cells and represent a unique lineage of immunoregulatory cells. J Immunol *160*, 1212-1218.

Takahashi, T., Kuniyasu, Y., Toda, M., Sakaguchi, N., Itoh, M., Iwata, M., Shimizu, J., and Sakaguchi, S. (1998). Immunologic self-tolerance maintained by CD25+CD4+ naturally anergic and suppressive T cells: induction of autoimmune disease by breaking their anergic/suppressive state. Int Immunol *10*, 1969-1980.

Takeuchi, J.K., Lou, X., Alexander, J.M., Sugizaki, H., Delgado-Olguin, P., Holloway, A.K., Mori, A.D., Wylie, J.N., Munson, C., Zhu, Y., Zhou, Y.Q., Yeh, R.F., Henkelman, R.M., Harvey, R.P., Metzger, D., Chambon, P., Stainier, D.Y., Pollard, K.S., Scott, I.C., and Bruneau, B.G. (2011). Chromatin remodelling complex dosage modulates transcription factor function in heart development. Nature communications *2*, 187.

Thornton, A.M., and Shevach, E.M. (1998). CD4+CD25+ immunoregulatory T cells suppress polyclonal T cell activation in vitro by inhibiting interleukin 2 production. J Exp Med *188*, 287-296.

Tone, Y., Furuuchi, K., Kojima, Y., Tykocinski, M.L., Greene, M.I., and Tone, M. (2008). Smad3 and NFAT cooperate to induce Foxp3 expression through its enhancer. Nat Immunol *9*, 194-202.

van Loosdregt, J., and Coffer, P.J. (2014). Post-translational modification networks regulating FOXP3 function. Trends Immunol *35*, 368-378.

van Loosdregt, J., Fleskens, V., Fu, J., Brenkman, A.B., Bekker, C.P., Pals, C.E., Meerding, J., Berkers, C.R., Barbi, J., Grone, A., Sijts, A.J., Maurice, M.M., Kalkhoven, E., Prakken, B.J., Ovaa, H., Pan, F., Zaiss, D.M., and Coffer, P.J. (2013). Stabilization of the transcription factor Foxp3 by the deubiquitinase USP7 increases Treg-cell-suppressive capacity. Immunity *39*, 259-271.

Wang, X., Wang, S., Troisi, E.C., Howard, T.P., Haswell, J.R., Wolf, B.K., Hawk, W.H., Ramos, P., Oberlick, E.M., Tzvetkov, E.P., Vazquez, F., Hahn, W.C., Park, P.J., and Roberts, C.W.M. (2019). BRD9 defines a SWI/SNF sub-complex and constitutes a specific vulnerability in malignant rhabdoid tumors. Nature communications *10*, 1881.

Webster, K.E., Walters, S., Kohler, R.E., Mrkvan, T., Boyman, O., Surh, C.D., Grey, S.T., and Sprent, J. (2009). In vivo expansion of T reg cells with IL-2-mAb complexes: induction of resistance to EAE and long-term acceptance of islet allografts without immunosuppression. J Exp Med *206*, 751-760.

Wildin, R.S., Ramsdell, F., Peake, J., Faravelli, F., Casanova, J.L., Buist, N., Levy-Lahad, E., Mazzella, M., Goulet, O., Perroni, L., Bricarelli, F.D., Byrne, G., McEuen, M., Proll, S., Appleby, M., and Brunkow, M.E. (2001). X-linked neonatal diabetes mellitus, enteropathy and endocrinopathy syndrome is the human equivalent of mouse scurfy. Nat Genet *27*, 18-20.

Wu, J.I., Lessard, J., Olave, I.A., Qiu, Z., Ghosh, A., Graef, I.A., and Crabtree, G.R. (2007). Regulation of dendritic development by neuron-specific chromatin remodeling complexes. Neuron *56*, 94-108.

Xue, Y., Canman, J.C., Lee, C.S., Nie, Z., Yang, D., Moreno, G.T., Young, M.K., Salmon, E.D., and Wang, W. (2000). The human SWI/SNF-B chromatin-remodeling complex is related to yeast rsc and localizes at kinetochores of mitotic chromosomes. Proceedings of the National Academy of Sciences of the United States of America *97*, 13015-13020.

Yan, Z., Cui, K., Murray, D.M., Ling, C., Xue, Y., Gerstein, A., Parsons, R., Zhao, K., and Wang, W. (2005). PBAF chromatin-remodeling complex requires a novel specificity subunit, BAF200, to regulate expression of selective interferon-responsive genes. Genes Dev *19*, 1662-1667.

Yang, X.O., Nurieva, R., Martinez, G.J., Kang, H.S., Chung, Y., Pappu, B.P., Shah, B., Chang, S.H., Schluns, K.S., Watowich, S.S., Feng, X.H., Jetten, A.M., and Dong, C. (2008). Molecular antagonism and plasticity of regulatory and inflammatory T cell programs. Immunity *29*, 44-56.

Yue, Y., Liu, J., and He, C. (2015). RNA N6-methyladenosine methylation in post-transcriptional gene expression regulation. Genes Dev *29*, 1343-1355.

Zhang, M., Chen, M., Kim, J.R., Zhou, J., Jones, R.E., Tune, J.D., Kassab, G.S., Metzger, D., Ahlfeld, S., Conway, S.J., and Herring, B.P. (2011). SWI/SNF complexes containing Brahma or Brahma-related gene 1 play distinct roles in smooth muscle development. Molecular and cellular biology *31*, 2618-2631.

Zhao, K., Wang, W., Rando, O.J., Xue, Y., Swiderek, K., Kuo, A., and Crabtree, G.R. (1998). Rapid and phosphoinositol-dependent binding of the SWI/SNF-like BAF complex to chromatin after T lymphocyte receptor signaling. Cell *95*, 625-636.

Zheng, Y., Josefowicz, S., Chaudhry, A., Peng, X.P., Forbush, K., and Rudensky, A.Y. (2010). Role of conserved non-coding DNA elements in the Foxp3 gene in regulatory T-cell fate. Nature *463*, 808-812.

Zhou, Y., Zhou, B., Pache, L., Chang, M., Khodabakhshi, A.H., Tanaseichuk, O., Benner, C., and Chanda, S.K. (2019). Metascape provides a biologist-oriented resource for the analysis of systems-level datasets. Nature communications *10*, 1523.